THEORETICAL STUDY OF A VISCOUS TURBINE

A THESIS

Presented to

The Faculty of the Division

of Graduate Studies

By   By

Ali Ihsan Yalcin

In Partial Fulfillment

of the Requirements for the Degree

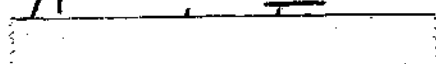Master of Science in Mechanical Engineering
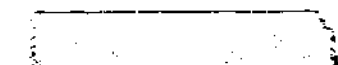
Georgia Institute of Technology

March, 1975

THEORETICAL STUDY OF A VISCOUS TURBINE

Approved:

Gene T. Colwell, Chairman

Thomas W. Jackson

C. W. Gorton

Date approved by Chairman: **3-5-75**

ACKNOWLEDGMENTS

I wish to express my gratitude to Dr. Gene T. Colwell for his valuable suggestions during the preparation of this thesis. His careful consideration of methods used and results obtained has assured the quality of this publication.

The School of Mechanical Engineering, Georgia Institute of Technology, made the analysis possible by generously financing the computer costs. I also wish to express my thanks to Dr. Thomas W. Jackson and Dr. C. W. Gorton for serving on my thesis committee.

TABLE OF CONTENTS

LIST OF TABLES

LIST OF ILLUSTRATIONS

GLOSSARY OF ABBREVIATIONS

A_t Nozzle throat or total slot inlet area, (ft^2)

g gravitational constant, $(lbm-ft/(lbf-sec^2))$

h height of a slot, (ft)

i,j,k peripheral, radial and axial directions, respectively

k ratio of specific heats

L,M,N number of increments on flow field in peripheral, radial and axial direction, respectively, as illustrated in Figure 6

$\dot{m}$ mass flow rate into slots (lbm/sec)

M_{No} nozzle throat or slot inlet Mach number

N_{Re} $\bar{\rho}_i \Omega w^2/\bar{\mu}_i$ = mechanical Reynolds number

$\bar{p}$ pressure, (F/L^2)

p $\bar{p}/(\bar{\rho}\Omega^2 R^2)$ = dimensionless pressure

$\bar{P}_o$ nozzle inlet stagnation pressure, (psf)

$\bar{P}_i$ slot inlet pressure (psf)

Q volume flow rate into slots, $(cu-ft/sec)$

r $\bar{r}/R$ = dimensionless radial length coordinate

R radius of wheel from center to the base of a slot (ft)

R_c universal gas constant, $(ft-lbf/(°R\ lbm-mole))$

$\bar{r}, \bar{z}$ radial and axial space coordinates, respectively, (L)

v_θ $\bar{v}_\theta/\Omega R$ = dimensionless peripheral velocity component

v_r $\bar{v}_r/\Omega h$ = dimensionless radial velocity component

v_z $\bar{v}_z/\Omega w$ = dimensionless axial velocity component

$\bar{v}_r, \bar{v}_\theta, \bar{v}_z$ radial, peripheral and axial velocity components, respectively, (L/T)

T_o nozzle inlet stagnation temperature, (°R)

w width of a slot, (ft)

z $\bar{z}/w$ = dimensionless axial length coordinate

Δr h/M = dimensionless radial space increment

$\Delta \theta$ Θ/L = dimensionless peripheral space increment

Δz z/N = dimensionless axial space increments

$\Delta v_\theta, \Delta v_r, \Delta v_z$ dimensionless incremental changes of peripheral, radial and axial velocity components between adjacent peripheral planes

Δp dimensionless incremental change of pressure across adjacent peripheral planes

$\bar{\mu}$ viscosity of fluid, (FT/L^2)

$\bar{\mu}_i$ slot inlet viscosity, $(lbm\text{-}sec/ft^2)$

μ $\bar{\mu}/\bar{\mu}_i$ = dimensionless viscosity

Ω angular velocity of wheel, (1/T)

ρ $\bar{\rho}/\bar{\rho}_i$ = dimensionless density

$\bar{\rho}$ density of fluid, (M/L^3)

$\bar{\rho}_o$ nozzle inlet stagnation density, (lbm/cu-ft)

$\bar{\rho}_i$ slot inlet density, (lbm/cu-ft)

$\bar{\theta}$ peripheral space coordinate (radians)

θ $\bar{\theta}/\Theta$ = dimensionless peripheral coordinate

Θ angle between nozzle exit and diffuser inlet with respect to center of wheel, (radians)

SUMMARY

Using a test rig, previously constructed in the School
of Mechanical Engineering, which modeled a viscous flow
compressor, Snit Dusadeenoad wrote a Master's Degree Thesis
on the "Characteristics of a Viscous Flow Compressor,"
September, 1970. Later a patent application on the "Turbine-
Compressor," was filed by Associate Professor Gene T. Colwell
and Professor Thomas W. Jackson, and U. S. Letters Patent
No. 3,751,908 was issued to the inventors on August 14, 1973.
At about the same time another Master's Degree Thesis was
presented by John S. Caldwell on "The Efficiency of a Viscous
Flow Compressor," June, 1973.

The present thesis analyzes the steady-state, adiabatic,
incompressible laminar flow of a fluid through compressor
side channels of a viscous type gas turbine by solving, on a
digital computer, the simplified three dimensional Navier-
Stokes equations of a flow field. Simplification of the
general set of equations was achieved by a dimensional
analysis of the problem. The order of magnitude difference
between the length dimensions made it possible to reduce the
complex Navier-Stokes equations into forms which could be
studied. The flow field was divided into a three dimensional
grid system. The simplified momentum and continuity equations
were applied at interior nodes of this grid system. The

non-linear partial differential equations were reduced to a set of algebraic linear equations by means of an indirect finite difference method. A suitable subroutine was selected from the digital computers's library to solve this set of equations in the most efficient manner. The mathematical model coupled with boundary and initial conditions made it possible to march the solution through the flow field until the exit section was reached.

The results obtained display velocity and pressure profiles for various operating conditions and geometric parameters. The effect of the centrifugal force field on the flow and the similarities between this problem and Couette flow are among the interesting results. Head rise versus flow rate curves have been plotted to enlighten the reader about the performance characteristics of this unique turbomachinery.

CHAPTER I

INTRODUCTION

1-1. The Viscous Drag Turbine

A turbine-compressor combustion engine of simple
construction with possible increased efficiency was designed
by Dr. Gene T. Colwell and Dr. Thomas W. Jackson and a
patent was issued for this invention (Reference 1). Also, a
rig was constructed in the School of Mechanical Engineering
of Georgia Institute of Technology. This rig enabled
experimental research on the compressor side of the design.
The results of these experiments were presented in references
5 and 6.

Momentum transfer between axially or radially moving
fluid stream and solid surfaces is reasonably well understood
in conventional turbomachinery. The machine under study in
this investigation, however, utilizes circumferentially
moving fluid streams in grooves radially cut into the
circumference of a rotating wheel. The fluid medium is
introduced through a nozzle cast into the housing. The walls
of each slot drag the fluid until it is stripped from the
wheel by seals which fit closely into the slots. The slots
are shown in Figures 1 and 2. If the inlet velocity of the
flow is less than the wheel tip speed, pressure builds up on
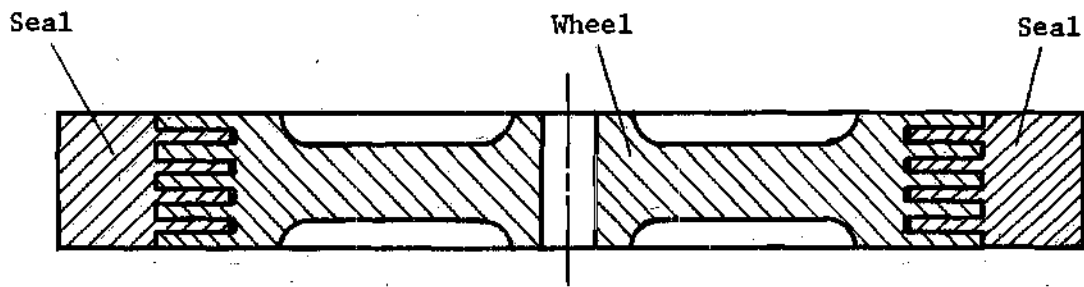
Figure 1. Wheel-Seal Assembly
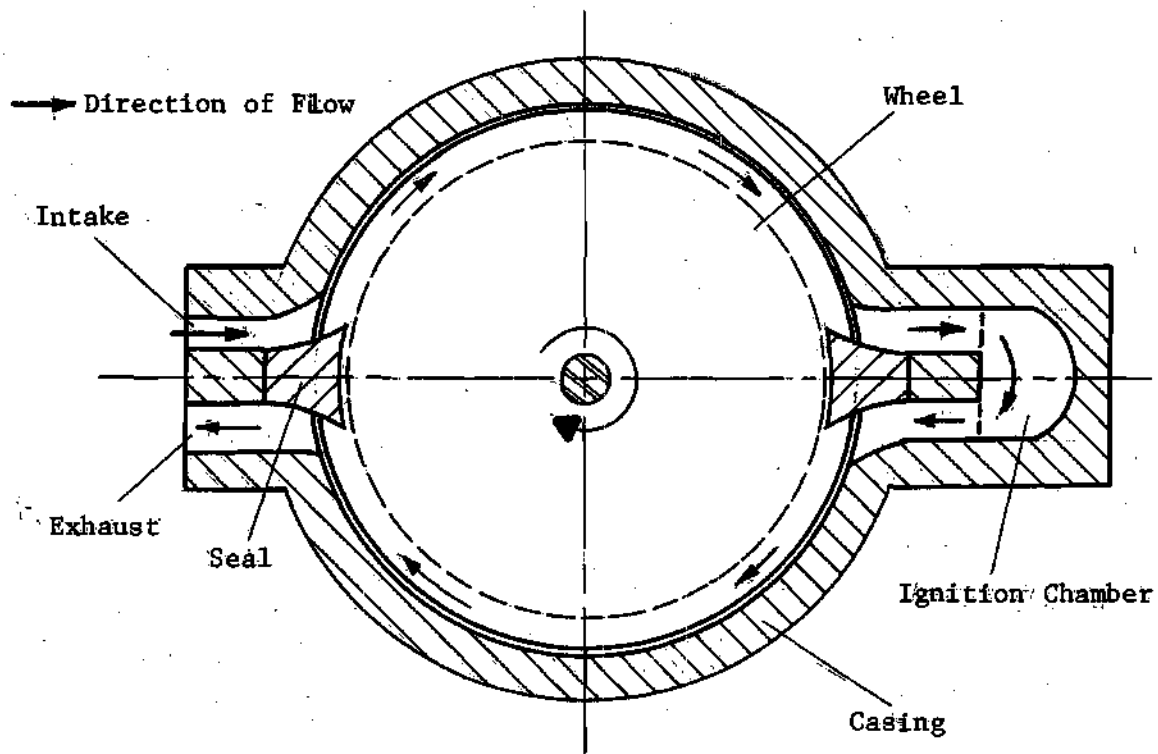
Figure 2. Viscous Drag Turbine

the compressor side. On the other hand, higher intake velocities by momentum exchange processes within the fluid drag the wheel and develop torque. Thus the same wheel is used as a compressor and turbine.

The discharge mechanism from the turbine is identical to that of the compressor side. While one side of the seals guide the fluid into the slots the other side scrapes it out of the grooves into a diffuser section. Flows with higher inlet velocities than wheel tip speeds are possible if compressed air is mixed in a combustion chamber with a stoichiometric fuel mixture, ignited and then discharged into the turbine side through a suitable nozzle. Feasible efficiencies are expected when the flow is turbulent within the wheel. Tip speeds exceeding the speed of sound for the intake fluid conditions are used with sonic limitations of flow to compress the medium more effectively. At stoichiometric temperatures the speed of sound is greater than the tip speed values and the fluid when fed back into the turbine side is able to expand freely.

An advantage of this design is the alternate cooling and heating of the slot walls in the compressor and turbine sides of the wheel. This eliminates the need for conventional blade cooling. Generally it is not desirable, from an efficiency standpoint, to heat during compression and or cool during expansion. However, the heat transfer in this case allows operation of the device at very high turbine inlet

temperatures without internal blade cooling. In addition, the heat transfer has a regenerative effect on the cycle. Thus the overall effect of the heat transfer is an increase in cycle performance.

1-2. Statement of the Problem

The goal of this project is to compute fluid velocity and pressure profiles in the slots of the viscous type gas turbine engine as described above. A laminar, steady, and incompressible solution of the three dimensional Navier-Stokes equationswwill be obtained for various geometries and operating conditions on the compressor side. In all real operating cases for the turbine under study, the flow will be turbulent. However, it is necessary to first study the laminar flow in this unique geometry.

Simplification of the general set of equations will be achieved by a dimensional analysis of the problem. The order of magnitude difference between the length dimensions will make it possible to reduce the complex Navier-Stokes equations into forms which can be studied. The flow field will be divided into a three dimensional grid system. The simplified momentum and continuity equations will be applied at interior modes of this grid system. The non-linear partial differential equations will be reduced to a set of algebraic linear equations by means of indirect finite difference method. The mathematical model coupled with

boundary and initial conditions will make it possible to march
the solution through the flow field until the exit section
is reached. Computations will be carried out in a digital
computer.

1-3. Literature Survey

The idea of utilizing fluid particles to drag surfaces
by viscous action was introduced by Nikolai Tesla [2] in the
early part of the century. However, due to the low effi-
ciencies at the rotational speeds used the study of flows
around rotating disks was considered to be an academic
exercise until recently.

The feasibility of using multiple-disk turbines in
special applications was recognized by researchers at the
Arizona State University. A thesis presented by Gordon [3]
and later a paper by Rice [4] indicate that such machinery
through less efficient than conventional turbomachinery shows
reasonably good efficiency values for small sizes. Since
multiple-disk turbines rely on wall shear stresses to convert
fluid power into mechanical torque, their performance is
independent of size whereas in conventional turbomachinery
viscous dissipation that increases by decreasing size is
considered to be a loss.

Literature on peripheral viscous drag compressors
became available after 1970 through the efforts of Dr. Gene T.
Colwell at Georgia Tech. Dusadeenoad [5] investigated the

adiabatic compression efficiency and head-flow characteristics of such machinery operating in the turbulent regime. He also presented a one dimensional analysis of the flow. For the force balance on an elemental control volume he made use of smooth pipe friction factor to approximate the wall shear stresses. The exit pressure was the dependent parameter of his set of equations. A thesis presented by Caldwell [6] displayed the importance of effective sealing on efficiency. His experiments were also conducted in turbulent regime.

Boyd and Rice [7] have considered the laminar flow of an incompressible Newtonian fluid, radially inward between parallel co-rotating disks. The through-flow was supported by an externally applied pressure difference between the outer periphery and a circular fluid exhaust hole at an inner radius. A sufficiently complete problem statement was formulated from the Navier-Stokes equations. Their problem had three parameters, a Reynolds number, a flow-rate parameter, and a peripheral tangential velocity component parameter.

In the present analysis extensive use has been made of the work of Schlichting [8] for the defining equations and the work of Batchelor [9] for information on dimensional analysis and the work of Shapiro [10] for isentropic flow formulas. Material presented by Roache [11] and Forsythe and Wasow [12] was utilized for applications of finite difference methods to partial differential equations. At FORTRAN IV programming phase of the problem Cracken [13] was utilized as

a frequent reference. A special problem presented by
Cantrell [14] at the Georgia Institute of Technology contained
valuable information which made certain assumptions possible
in this analysis.

CHAPTER II

THEORETICAL DEVELOPMENT

2-1. Defining Equations

The governing set of equations for a fluid flowing through the compressor-turbine should be in cylindrical coordinates for ease in computations. The one dimensional analysis of laminar flow by Cantrell [13] through the same geometry suggests that the flow field is incompressible and isothermal. Under these conditions steady state Navier-Stokes equations in cylindrical coordinates are:

r-momentum equation,

$$\bar{\rho}(\bar{v}_r \frac{\partial \bar{v}_r}{\partial \bar{r}} + \frac{\bar{v}_\theta}{\bar{r}} \frac{\partial \bar{v}_r}{\partial \bar{\theta}} - \frac{\bar{v}_\theta^2}{\bar{r}} + \bar{v}_z \frac{\partial \bar{v}_r}{\partial \bar{z}}) = - \frac{\partial \bar{p}}{\partial \bar{r}} + \bar{\mu}[\frac{\partial}{\partial \bar{r}}(\frac{1}{\bar{r}} \frac{\partial}{\partial \bar{r}}(\bar{r}\bar{v}_r))$$

$$+ \frac{1}{\bar{r}^2} \frac{\partial^2 \bar{v}_r}{\partial \bar{\theta}^2} - \frac{2}{\bar{r}^2} \frac{\partial \bar{v}_\theta}{\partial \bar{\theta}} + \frac{\partial^2 \bar{v}_r}{\partial \bar{z}^2}] \; ;$$

θ-momentum equation,

$$\bar{\rho}(\bar{v}_r \frac{\partial \bar{v}_\theta}{\partial \bar{r}} + \frac{\bar{v}_\theta}{\bar{r}} \frac{\partial \bar{v}_\theta}{\partial \bar{\theta}} + \frac{\bar{v}_r \bar{v}_\theta}{\bar{r}} + \bar{v}_z \frac{\partial \bar{v}_\theta}{\partial \bar{z}} = - \frac{1}{\bar{r}} \frac{\partial \bar{p}}{\partial \bar{\theta}} + \bar{\mu}[\frac{\partial}{\partial \bar{r}}(\frac{1}{\bar{r}} \frac{\partial}{\partial \bar{r}}(\bar{r}\bar{v}_\theta))$$

$$+ \frac{1}{\bar{r}^2} \frac{\partial^2 \bar{v}_\theta}{\partial \bar{\theta}^2} + \frac{2}{\bar{r}^2} \frac{\partial \bar{v}_r}{\partial \bar{\theta}} + \frac{\partial^2 \bar{v}_\theta}{\partial \bar{z}^2}] \; ;$$

z-momentum equation,

$$\bar{\rho}(\bar{v}_r \frac{\partial \bar{v}_z}{\partial \bar{r}} + \frac{\bar{v}_\theta}{\bar{r}} \frac{\partial \bar{v}_z}{\partial \bar{\theta}} + \bar{v}_z \frac{\partial \bar{v}_z}{\partial \bar{z}}) = - \frac{\partial \bar{p}}{\partial \bar{z}} + \bar{\mu}[\frac{1}{\bar{r}} \frac{\partial}{\partial \bar{r}} (\bar{r} \frac{\partial \bar{v}_z}{\partial \bar{r}})$$

$$+ \frac{1}{\bar{r}^2} \frac{\partial^2 \bar{v}_z}{\partial \bar{\theta}^2} + \frac{\partial^2 \bar{v}_z}{\partial \bar{z}^2}] \ .$$

The flow has to satisfy the equation for conservation
of mass in cylindrical coordinates for an incompressible
fluid at steady state.

$$\frac{1}{\bar{r}} (\frac{\partial}{\partial \bar{r}} (\bar{r} \bar{v}_r)) + \frac{1}{\bar{r}} (\frac{\partial \bar{v}_\theta}{\partial \bar{\theta}}) + \frac{\partial v_z}{\partial \bar{z}} = 0 .$$

The above four equations will be accompanied by
boundary conditions that describe the geometry under study.
The geometry is illustrated in Figure 4. A characteristic
of the geometry which reduces the possible number of unknowns
and computational time is the axial symmetry across the
centerline of a slot. Also the flow along each slot will
be assumed to be identical so that total flow through the
field is simply a sum of flows through the individual slots.
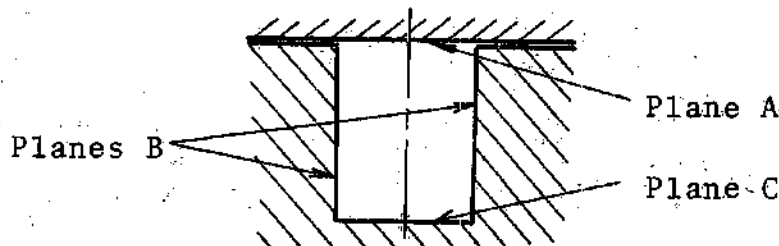
Figure 3. Slot Nomenclature
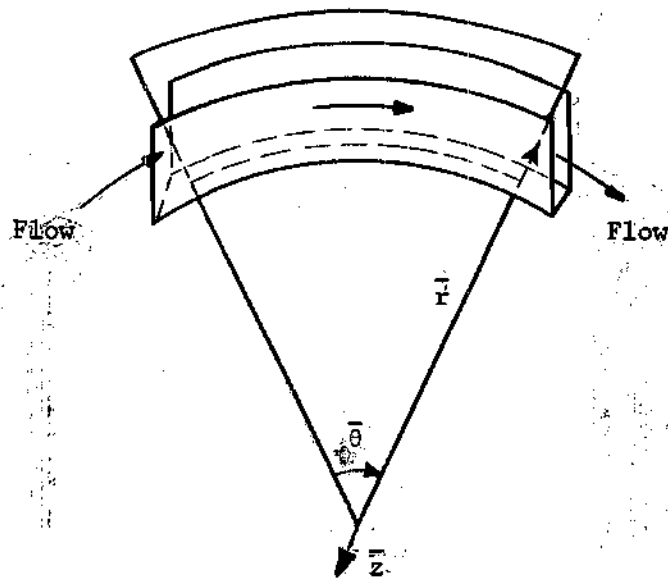
Figure 4. The Coordinate System

According to the figure above the boundary conditions are:

$\overline{v}_\theta = \Omega \overline{r}$ on planes B and C

$\overline{v}_\theta = 0$ on plane A

$\overline{v}_z = 0$ on planes A, B, C and centerline

$\overline{v}_r = 0$ on planes A, B, C

$\dfrac{\partial \overline{v}_\theta}{\partial \overline{z}}\Big|_k = 0$ due to symmetry

$\dfrac{\partial \overline{v}_r}{\partial \overline{z}}\Big|_k = 0$ due to symmetry

$\dfrac{\partial \overline{v}_z}{\partial \overline{z}} = 0$ on planes B

$\overline{v}_\theta = v_{in}, \; \overline{v}_z = 0, \; \overline{v}_r = 0$ at inlet

That this set of equations is enough to define the problem completely will be shown later on when finite difference forms of equations are developed.

2-2. Dimensional Analysis

The variables involved are non-dimensionalized by characteristic quantities such that the resulting quotients are of order one. To facilitate the order of magnitude analysis, the depth of slot to wheel radius ratio, h/R, and width of slot to wheel radius ratio, w/R, are assumed to be

much less than one. For detailed developments of non-dimensional Navier-Stokes equations and the equation of continuity see Appendix A. The resulting equations are as follows:

Continuity,

$$\frac{1}{\Theta} \frac{\partial v_\theta}{\partial \theta} + r \frac{\partial v_z}{\partial z} = 0 \; ;$$

r-momentum equation,

$$- \frac{v_\theta^2}{r} = - \frac{\partial p}{\partial r} + (\frac{h}{R}) (\frac{1}{N_{Re}}) \frac{\partial^2 v_r}{\partial z^2} \; ;$$

θ-momentum equation,

$$\frac{1}{\Theta} \frac{v_\theta}{r} \frac{\partial v_\theta}{\partial \theta} + v_z \frac{\partial v_\theta}{\partial z} = - \frac{1}{\Theta} \frac{\partial p}{r \partial \theta} + (\frac{1}{N_{Re}}) (\frac{\partial^2 v_\theta}{\partial z^2}) \; ; \quad \text{and}$$

z-momentum equation,

$$\frac{\partial p}{\partial z} = 0.$$

Boundary conditions are:

$$v_\theta = 0 \qquad \text{on plane A,}$$
$$v_\theta = r \qquad \text{on plane B,}$$

$v_\theta = 1$ on plane C,

$v_z = 0$ on planes A, B, C and centerline,

$v_r = 0$ on planes A, B and C,

$\dfrac{\partial v_\theta}{\partial z} = 0$ on centerline,

$\dfrac{\partial v_z}{\partial z} = 0$ on plane B, and

$\dfrac{\partial v_r}{\partial z} = 0$ on centerline.

The non-dimensional momentum equations when analyzed term by term yield relevant information about the flow. The radial momentum equation sets a balance between radial pressure gradients and centrifugal forces plus an order of magnitude smaller radial viscous force term retained for mathematical compatibility. If the inertial terms on the left hand side of the θ-momentum equation are reorganized by utilizing the continuity equation, the result is,

$$\frac{1}{\Theta}\frac{\partial v_\theta^2}{r\partial\theta} + \frac{\partial(v_\theta v_z)}{\partial z} = -\frac{1}{\Theta}\frac{\partial p}{r\partial\theta} + \frac{1}{N_{Re}}\left(\frac{\partial^2 v_\theta}{\partial z^2}\right).$$

The physical interpretation is that the change in θ-momentum carried peripherally plus that carried axially is equal to the peripheral pressure gradient plus the viscous force gradient in the same direction. Note that, when the flow is fully developed, this equation defines the familiar Couette flow problem. The axial momentum equation shows that the axial pressure gradient in the flow is negligible,

resembling the well-known flat-plate boundary layer approximation.

The inlet conditions are specified as zero approach velocity into the nozzle and slug-type flow into the grooves. The nozzle throat area is set equal to the total cross-sectional slot area. When the Mach number at the nozzle throat or at the inlet to the grooves, the area, and nozzle inlet stagnation conditions are specified, the mass flow rate, slot inlet static pressure, and density can be computed along with volume flow rate as an end product by the following formulas obtained from Reference 9. An illustration of the development of meridnnial velocity profiles starting from nozzle inlet section until the diffuser exit is given on Figure 5.

$$\dot{m} = A_t \sqrt{\frac{kg}{R_c}} \left(\frac{\bar{P}_o}{\sqrt{T_o}}\right) \frac{M}{\frac{(1+\frac{(k-1)}{2}M_{No}^2)}{(1+\frac{(k-1)}{2}M_{nod}^2)}\left(\frac{k+1}{2(k-1)}\right)}$$

$$\bar{P}_i = \bar{P}_o / (1 + \frac{k-1}{2} M_{No}^2)^{\frac{k}{k-1}}$$

$$\bar{\rho}_i = \bar{\rho}_o / (1 + \frac{k-1}{2} M_{No}^2)^{\frac{1}{k-1}}$$

$$Q = \dot{m}/\bar{\rho}_i$$

Nozzle

Wheel

Diffuser
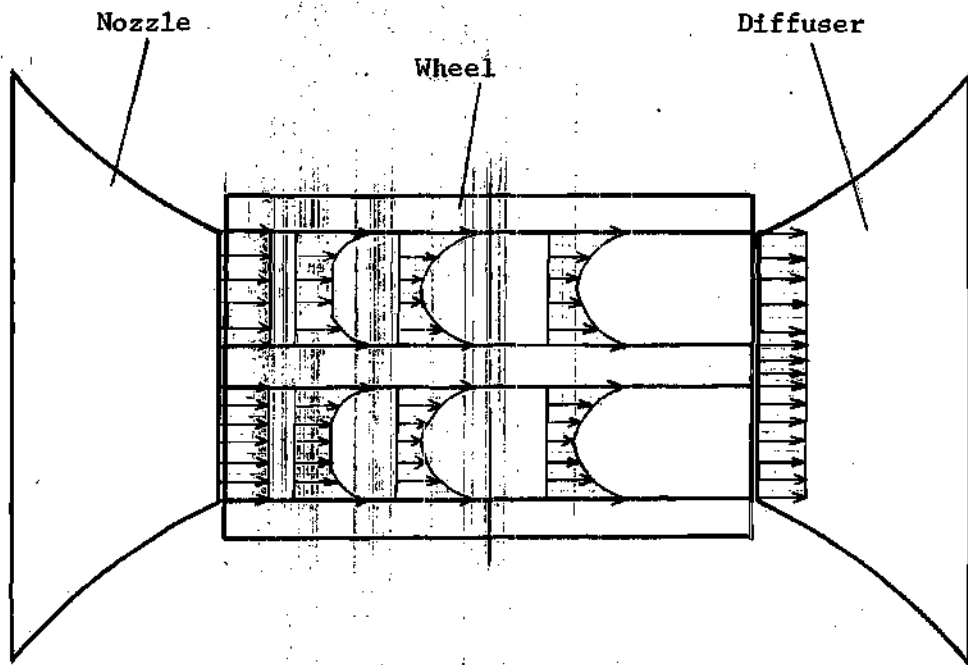
Figure 5.   Schematic Meridonial Velocity Development

At the exit of the slots it is necessary to perform an averaging process by double integration over the area to determine the peripheral velocity component. Exit pressure should be subjected to an averaging process over a line since it is only dependent on radial directions across a radial plane.

In the diffuser section the mean values will be used in similar equations to those that govern the flow through the nozzle to determine final exit pressure.

2-3. Application of Numerical Techniques

There are various methods to solve the above described sets of equations and related boundary and initial conditions. As suggested in Reference 7, a means of linearizing them into a form suitable to digital computer treatment was pursued. Due to the tangential symmetry in Reference 7 it was possible to omit tangential derivatives from the set of governing equations. In the present analysis the flow field develops in the tangential direction so tangential derivatives are essential. Compared to the parabolic inlet flow conditions of Reference 7 this analysis assumes slug-type inlet flow conditions. Also, Reference 7 uses a non-uniform grid spacing in radial direction whereas this study considers uniform grid spacing at inlet and fully developed flow sections to be sufficiently accurate.

The slot in which the fluid flows was divided into

L-segments in the peripheral direction from nozzle to diffuser, M-radial stations from the base of a slot to the shroud, and N-sections from the center of a slot to the moving wall on either side of it. A complete illustration of the lattice is shown in Figure 6.

Initially, defining equations are approximated by a finite difference scheme such that all variables assume their values at the next peripheral station. Tangential derivatives utilize backward difference schemes whereas all others are approximated by centered difference methods. A sample derivation for the θ-momentum equation is given in Appendix E. In light of these measures the equations became:

Equation of continuity,

$$\frac{v_\theta(i+1,j,k)-v_\theta(i,j,k)}{\theta\Delta\theta} + r_j \frac{v_z(i+1,j,k+1)-v_z(i+1,j,k-1)}{2\Delta z} = 0;$$

r-momentum equation,

$$-\frac{1}{r_j}(v_\theta(i+1,j,k))^2 = -\frac{p(i+1,j+1)-p(i+1,j-1)}{2\Delta r} +$$

$$(\frac{h}{R})(\frac{1}{N_{Re}})(\frac{v_r(i+1,j,k+1)-2v_r(i+1,j,k)+v_r(i+1,j,k-1)}{(\Delta z)^2}); \text{ and}$$

j=M
j=M-1
j=M-2

B

B

j=3
j=2
j=1

i=3
i=2
i=1

i=L-1
i=L

j=M

k=1 k=2 k=3

k=N

j=M-1

k=N-1

j=3
j=2
j=1

Section B-B
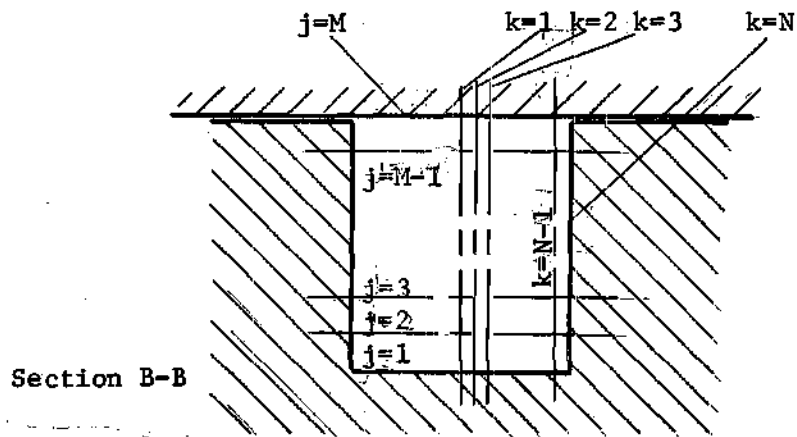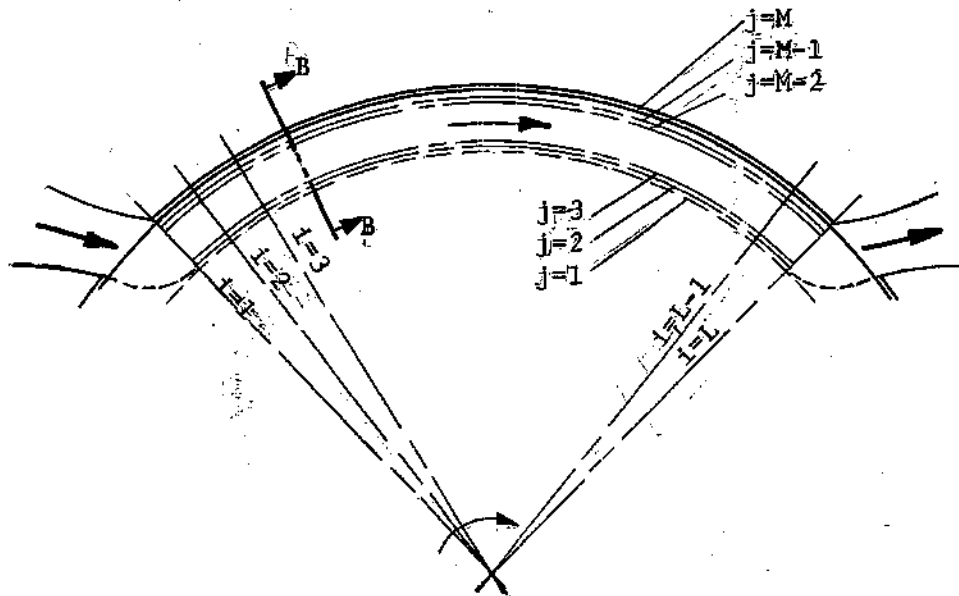
Figure 6.   Orientation of Grid Spacing on the Geometry

θ-momentum equation,

$$\frac{v_\theta(i+1,j,k)}{r_j} \frac{v_\theta(i+1,j,k)-v_\theta(i,j,k)}{\theta\Delta\theta} +$$

$$v_z(i+1,j,k)\frac{v_\theta(i+1,j,k+1)-v_\theta(i+1,j,k-1)}{2\Delta z} =$$

$$\frac{p(i+1,j)-p(i,j)}{r_j\theta\Delta\theta} + \frac{1}{N_{Re}}[\frac{v_\theta(i+1,j,k+1)-2v_\theta(i+1,j,k)+v_\theta(i+1,j,k-1)}{(\Delta z)^2}].$$

Boundary conditions,are:

$v_\theta(i+1,M,k) = 0$

$v_\theta(i+1,j,N) = r_j$

$v_z(i+1,j,1) = v_z(i+1,j,N) = v_z(i+1,1,k) = v_z(i+1,M,k) = 0$

$v_r(i+1,j,N) = v_r(i+1,1,k) = v_r(i+1,M,k) = 0$

$3v_\theta(i+1,j,1)-4v_\theta(i+1,j,2)+v_\theta(i+1,j,3) = 0$

$3v_z(i+1,j,N)-4v_z(i+1,j,N-1)+v_z(i+1,j,N-2) = 0$

$7v_r(i+1,j,1)-8v_r(i+1,j,2)+v_r(i+1,j,3) = 0$

The z-momentum equationssrseeaitiis incorporated into the above equations by setting pressure variables independent of axial gradients. The fact that the above equations are still non-linear means that they are very difficult to solve directly. To overcome this problem a new set of variables are introduced:

$$\Delta v(j,k) = v(i+1,j,k) - v(i,j,k)$$

$$\Delta v_z(j,k) = v_z(i+1,j,k) - v_z(i,j,k)$$

$$\Delta v_r(j,k) = v_r(i+1,j,k) - v_r(i,j,k)$$

$$\Delta p(j) = p(i+1,j) - p(i,j).$$

Substituting the variables into the equations and neglecting any term that contains products of the variables which are small, i.e. the following set of equations and boundary conditions:

Equation of continuity,

$$2\left(\frac{\Delta z}{\theta r_j \Delta \theta}\right)\Delta v_\theta(j,k) - \Delta v_z(j,k-1) + \Delta v_z(j,k+1) = v_z(i,j,k-1) - v_z(i,j,k+1);$$

r-momentum equation,

$$- \left(\frac{2}{r_j}\right)\left(\frac{R\Delta z}{h}\right)(v_\theta(i,j,k))\Delta v_\theta(j,k) - \left(\frac{1}{N_{Re}\Delta z}\right)\Delta v_r(j,k-1) + \left(\frac{2}{N_{Re}\Delta z}\right)$$

$$\Delta v_r(j,k) - \left(\frac{1}{N_{Re}\Delta z}\right)\Delta v_r(j,k+1) + g\left(\frac{1}{2\Delta r}\right)\left(\frac{R\Delta z}{h}\right)\Delta p(j+1) - g$$

$$\left(\frac{1}{2\Delta r}\right)\left(\frac{R\Delta z}{h}\right)\Delta p(j-1) = \left(\frac{1}{r_j}\right)\left(\frac{R\Delta z}{h}\right)(v_\theta(i,j,k))^2 - g\left(\frac{1}{2\Delta r}\right)\left(\frac{R\Delta z}{h}\right)$$

$$(p(i,j+1) - p(i,j-1)) + \left(\frac{1}{N_{Re}\Delta z}\right)(v_r(i,j,k+1) - 2v_r(i,j,k) + v_r(i,j,k-1));$$

and

θ-momentum equation,

$$[-(\frac{1}{N_{Re}\Delta z})-0.5\ v_z(i,j,k)]\Delta v_\theta(j,k-1)+[(\frac{\Delta z}{\Theta\Delta\theta r_j})v_\theta(i,j,k)\ +$$

$$2(\frac{1}{N_{Re}\Delta z})]\Delta v_\theta(j,k)+[0.5\ v_z(i,j,k)-\frac{1}{N_{Re}\Delta z}]\Delta v_\theta(j,k+1)\ +$$

$$[0.5(v_\theta(i,j,k+1)-v_\theta(i,j,k-1))]\Delta v_z(j,k)+g[\frac{\Delta z}{\Theta r_j\Delta\theta}]\Delta p(j)\ =$$

$$(\frac{1}{N_{Re}\Delta z})(v_\theta(i,j,k+1)-2v_\theta(i,j,k)+v_\theta(i,j,k-1))\ -$$

$$0.5\ v_z(i,j,k)(v_\theta(i,j,k+1)-v_\theta(i,j,k-1)).$$

Boundary conditions are

$\Delta v_\theta(j,N)\ =\ r_j-v_\theta(i,j,N)$

$\Delta v_\theta(M,k)\ =\ 0$

$\Delta v_z(j,1)\ =\ \Delta v_z(j,N)\ =\ \Delta v_z(M,k)\ =\ \Delta v_z(1,k)\ =\ 0$

$\Delta v_r(j,N)\ =\ \Delta v_r(M,k)\ =\ \Delta v_r(1,k)\ =\ 0$

$3\Delta v_\theta(j,1)-4\Delta v_\theta(j,2)+\Delta v_\theta(j,3)\ =\ -3v_\theta(i,j,1)+4v_\theta(i,j,2)-v_\theta(i,j,3)$

$\Delta v_z(j,N-2)-4\Delta v_z(j,N-1)\ =\ -v_z(i,j,N-2)+4v_z(i,j,N-1)$

$$7 \Delta v_r(j,1) - 8 \Delta v_r(j,2) + \Delta v_r(j,3) = -7v_r(i,j,1) + 8v_r(i,j,2) - v_r(i,j,3).$$

Equations of continuity and momentum are applied to the internal nodes on a peripheral plane. Boundary conditions are defined at lattice points on the boundaries. Since shroud and base of the groove pressures are unknown, the radial gradient is expanded in a forward difference or a backward difference method in the radial direction depending upon whether the node is on an axial plane next to the base of the groove or on the last one before the shroud, respectively.

After this special treatment the number of unknowns on any particular peripheral plane is $3(M-2)(N-1)$. Owing to symmetry and known values of certain variables on the solid boundaries and centerline, the number of unknowns has been substantially decreased.

Upon careful investigation of the equations and boundary conditions it is evident they constitute a set of linear algebraic equations that can be fitted into the format below:

$$\{A\}[X] = [C]$$

where matrix A contains the coefficients of the variables involved, X is a vector composed of $3(M-2)(N-1)$ unknown Δ variables and C is a constant vector that includes all

elements that are on the right of the equality sign of the equations.

The reason why the elements in vectors A and C are known is that they are composed of quantities that are either geometric parameters, system characteristics, and/or variables calculated or known from previous computations or by initial conditions.

Among the various methods of solution of a linear system of equations, Gaussian elimination is particularly suitable in the present case because matrix A is sparse; that is, the rows and the columns have considerable amounts of zero elements. This type of solution format was available in the Georgia Institute of Technology Computer Center Library in subroutine form.

The principle of solution is to reduce matrix A into a triangular system by a series of divisions and subtractions. The set of equations are originally in the form below,

$$a_{11}x_1 + a_{12}x_2 + \cdots + a_{1,n-1}x_{n-1} + a_{1,n}x_n = c_1$$

$$a_{21}x_1 + a_{22}x_2 + \cdots + a_{2,n-1}x_{n-1} + a_{2,n}x_n = c_2$$

$$\vdots \qquad \vdots \qquad \qquad \vdots \qquad \qquad \vdots \qquad \vdots$$

$$a_{n}x_1 + a_{n,2}x_2 + \cdots + a_{n,n-1}x_{n-1} + a_{n,n}x_n = c_n$$

The first equation is initially divided by a_{11} (assuming that $a_{11} \neq 0$) and the result is used to eliminate x_1 from all succeeding equations. Next, the modified second equation is divided by the coefficient of x_2 in that equation and the result is used to eliminate x_2 from the succeeding equations, and so forth. After this elimination process has been effected n-times, the resultant set, which is equivalent to the original one except for the effect of any round-offs committed, is of the form

$$x_1 + a'_{1,2}x_2 + \ldots + a'_{1,n}x_n = c'_1$$

$$x_2 + \ldots + a'_{2,n}x_n = c'_2$$

$$\vdots \qquad \vdots$$

$$x_{n-1} + a'_{n-1,n}x_n = c'_{n-1}$$

$$x_n = c'^{'}_n$$

where $a'_{i,j}$, c'_i designate specific numerical values. The solution is completed by working backwards from the last equation, to obtain successively x_n, $x_{n-1}, \ldots, x_1$.

Solving the linear system of equations with the method cited above yields the unknown Δ-variables. Δ-variables, by definition, are differences in magnitude of velocity components or pressure between consecutive peripheral planes

such that the value on the first plane is always known by
inlet conditions or previous similar calculations. Thus,
Δ-variables yield, indirectly, velocity components and
pressures on each node of a peripheral plane.

For the next set of calculations a similar matrix is
set up and the coefficients and constant matrix elements are
calculated with inclusion of new velocity components and
pressures. This logic is followed until the exit stage is
reached. The computer logic behind the method of solution
is presented in Figure 7.

The axial and radial variations of the peripheral
velocity are averaged by using Simpson's one-third rule for
double integration to get the mean exit velocity. Subsequent
checks of the accuracy of the computations are made by
calculating the mass flow rate which should, ideally, be
conserved. If the increments in the radial direction are
chosen to be equal, the average exit pressure can be computed
by a simple arithmetic mean.
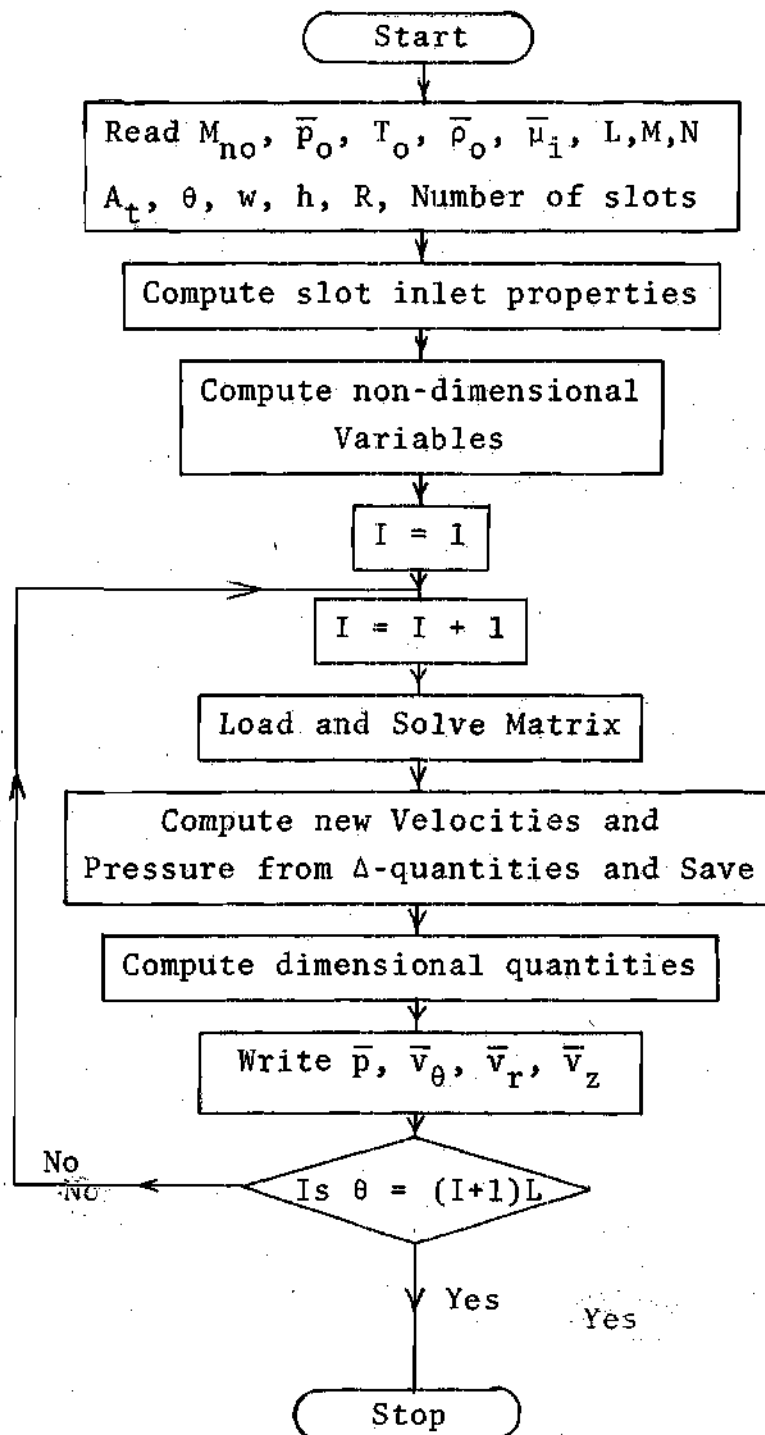
Figure 7. Computer Block Flow Diagram

CHAPTER III

RESULTS

3-1. Range of Parameters

To obtain meaningful results from the set of equations
and boundary conditions discussed in the previous section,
the flow regime must necessarily be of a laminar nature. If
the Reynolds number based on the relative fluid velocity and
hydraulic radius is less than 2000 it may be assumed that the
flow is laminar on grounds that the flow field is similar
to that in non-circular pipes. Since incompressible and
isothermal flow conditions were assumed, by setting density
and viscosity equal to constant values, the constraint on
Reynold's number as stated above results in important
relations between wheel angular velocity, fluid absolute
velocity, wheel radius, and slot width.

If,

$$Re = \frac{\overline{\rho}(\Omega R - v_\theta(1,j,k))D_H}{\overline{\mu}} < 2000$$

and,

$$D_H = 4\left(\frac{hw}{2h+2w}\right) \simeq 2w$$

with conditions,

$$\overline{\rho} = 0.075 \text{ lbm/cu.ft.}$$

$$\overline{\mu} = 0.000012 \text{ lbm/ft.sec.}$$

$$w = 0.05 \text{ inch}$$

then,

then,

$$\Omega < \frac{v_\theta(1,j,k)}{R} + \frac{0.16}{wR} \quad \text{and} \quad \Omega R > v_\theta(1,j,k)$$

Parameters of prime importance are the mechanical Reynolds number, inlet velocity, and slot height to wheel diameter ratio since they appear as coefficients in the defining equations or as inlet conditions. To be able to obtain meaningful head rise versus flow rate curves for compressor operation, either mechanical Reynolds number or slot height to wheel diameter ratio has to be kept constant and the other varied. For this purpose the scheme as shown in Table 2 has been used.

3-2. Evaluation of Outputs

It is easier to derive meaningful conclusions from the dimensional results if they are plotted on graphs.

Table 1.   Possible Limits of Inlet Velocity Under
Various Operating Conditions

R (inches)	w (inch)	Ω(rpm)		
		1000	1500	2000
3.5	0.05	Not possible	$7 < v_{in} < 46$	$27 < v_{in} < 62$
3.5	0.08	$7 < v_{in} < 31$	$18 < v_{in} < 46$	$37 < v_{in} < 62$
5.0	0.05	$5 < v_{in} < 44$	$27 < v_{in} < 65$	$49 < v_{in} < 88$
5.0	0.08	$20 < v_{in} < 44$	$41 < v_{in} < 65$	$63 < v_{in} < 88$

Table 2.   Data Layout for Fifteen Runs

Ω (rpm)	w (inch)	R (inches)	h (inch)	$v_\theta(1,j,k)$(ft/sec)		
				a	b	c
1000	0.05	5.0	0.5	10	25	40
1500	0.05	5.0	0.5	30	43	60
2000	0.05	5.0	0.5	55	65	75
1500	0.05	3.5	0.5	15	25	40
1500	0.05	7.0	0.5	60	70	80

Figures 8 and 9 display the development of tangential velocity profiles from the inlet section up to the fully developed section for runs with the same inlet velocities but different tip speeds. Figures 9 and 10 illustrate the development of tangential velocity profiles of cases with same tip speeds but different inlet velocities. The computer program was designed such that when the increment between tangential velocities on adjacent peripheral planes decreased to a limiting value, a trigger mechanism is activated to kick the peripheral mesh size to smaller values. This marks the beginning of fully developed region. Figures 8, 9, and 10 show that as the relative fluid velocity between wheel tip speed and inlet velocity is increased, it takes longer for the fluid flow to become fully developed. The steeper tangential velocity gradients on the moving walls in Figures 8 and 10 compared to Figure 9 mean that the fluid flow is sheared more at higher relative velocities. The backfflow in Figure 10 at 3.5 degrees away from the inlet has an interesting influence on the pressure gradient at the same section. This phenomenon will be discussed later.

Figure 11 displays a centerline tangential velocity distribution along the radius at various distances from the inlet. The end points of the profiles have been marked with dashed lines since the boundary conditions on the shroud and on the base of the groove have not been included into the calculations. This is understandable because radial shearing

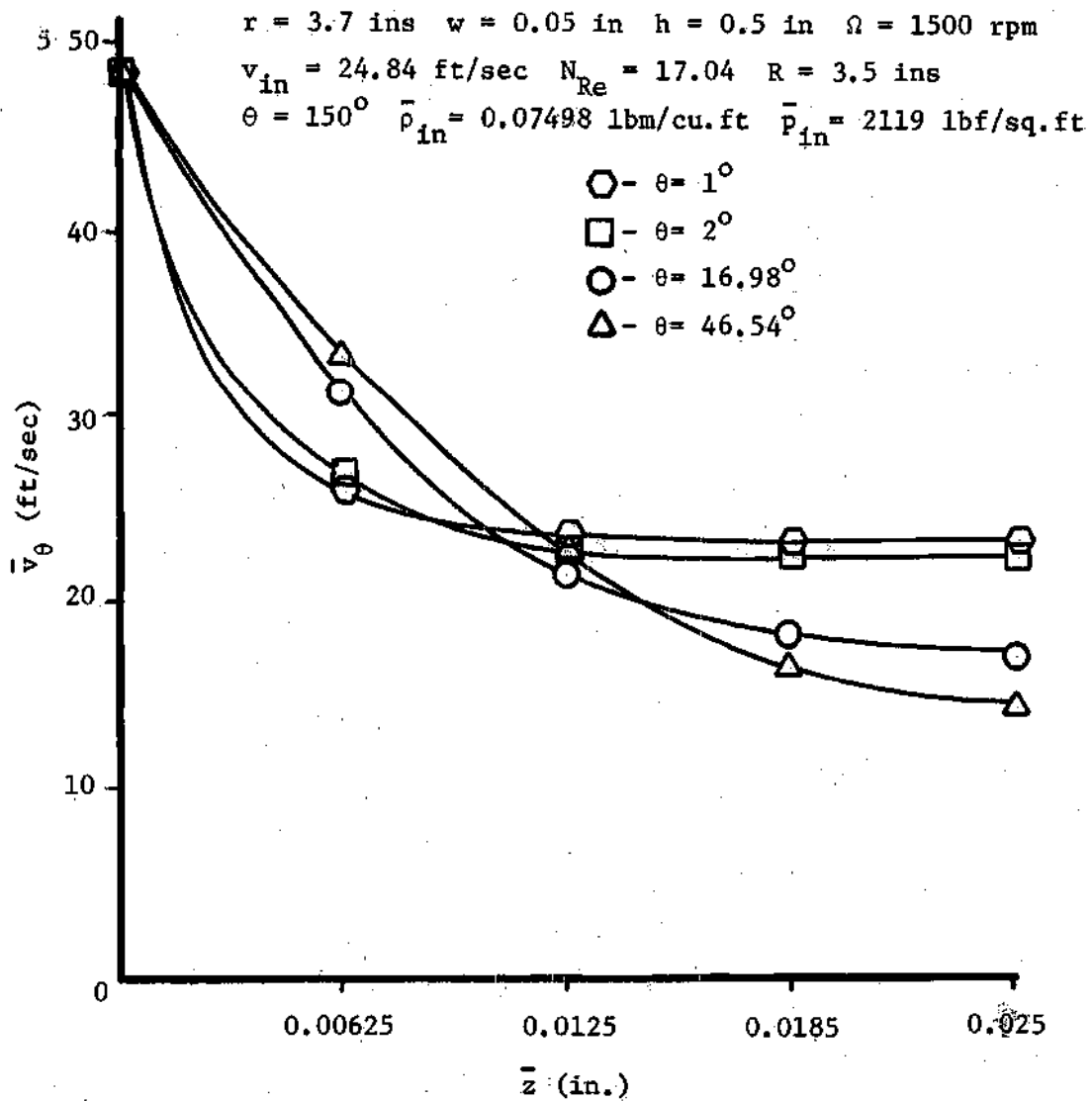Figure 8. Tangential Velocity Profile Development

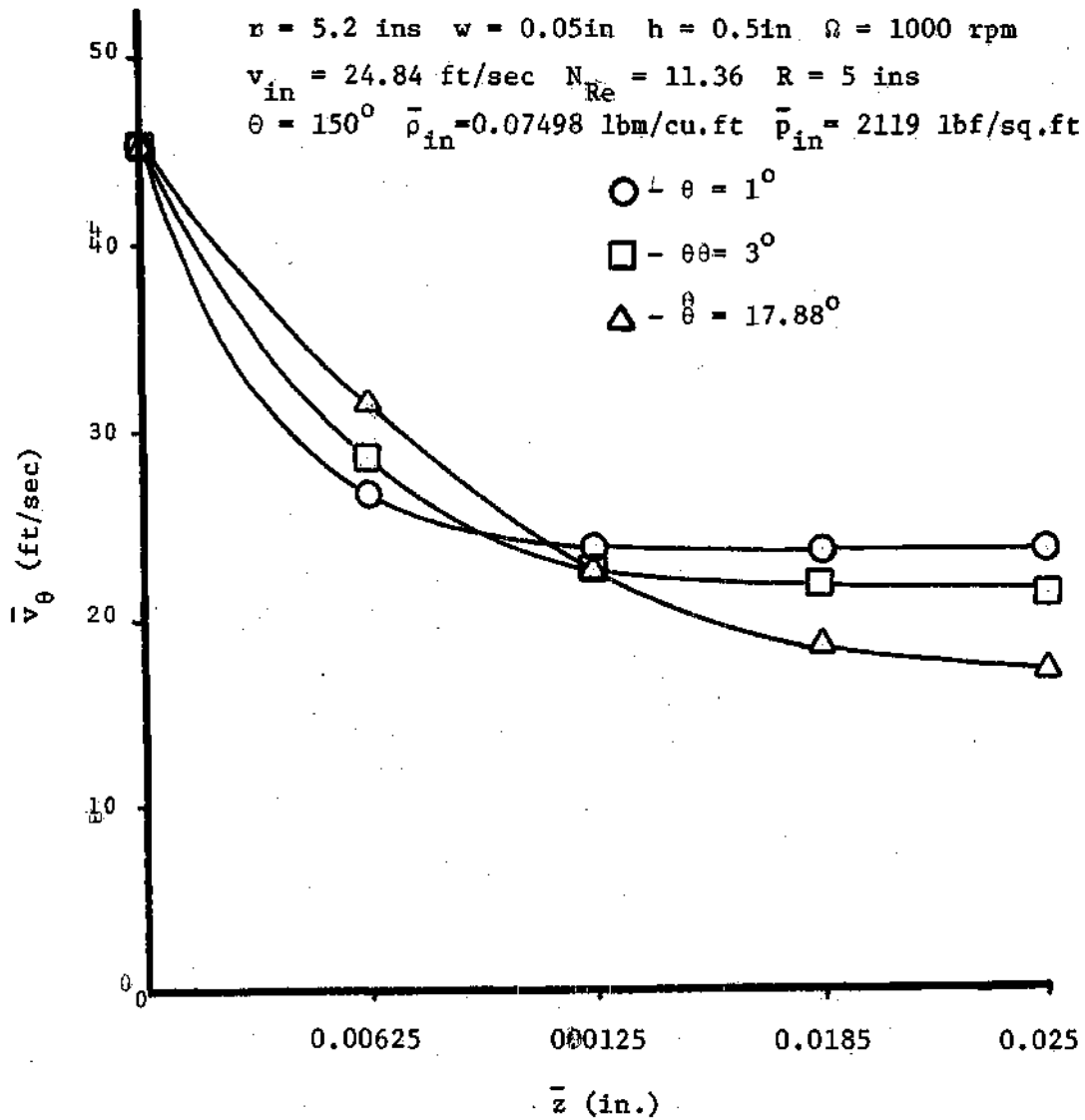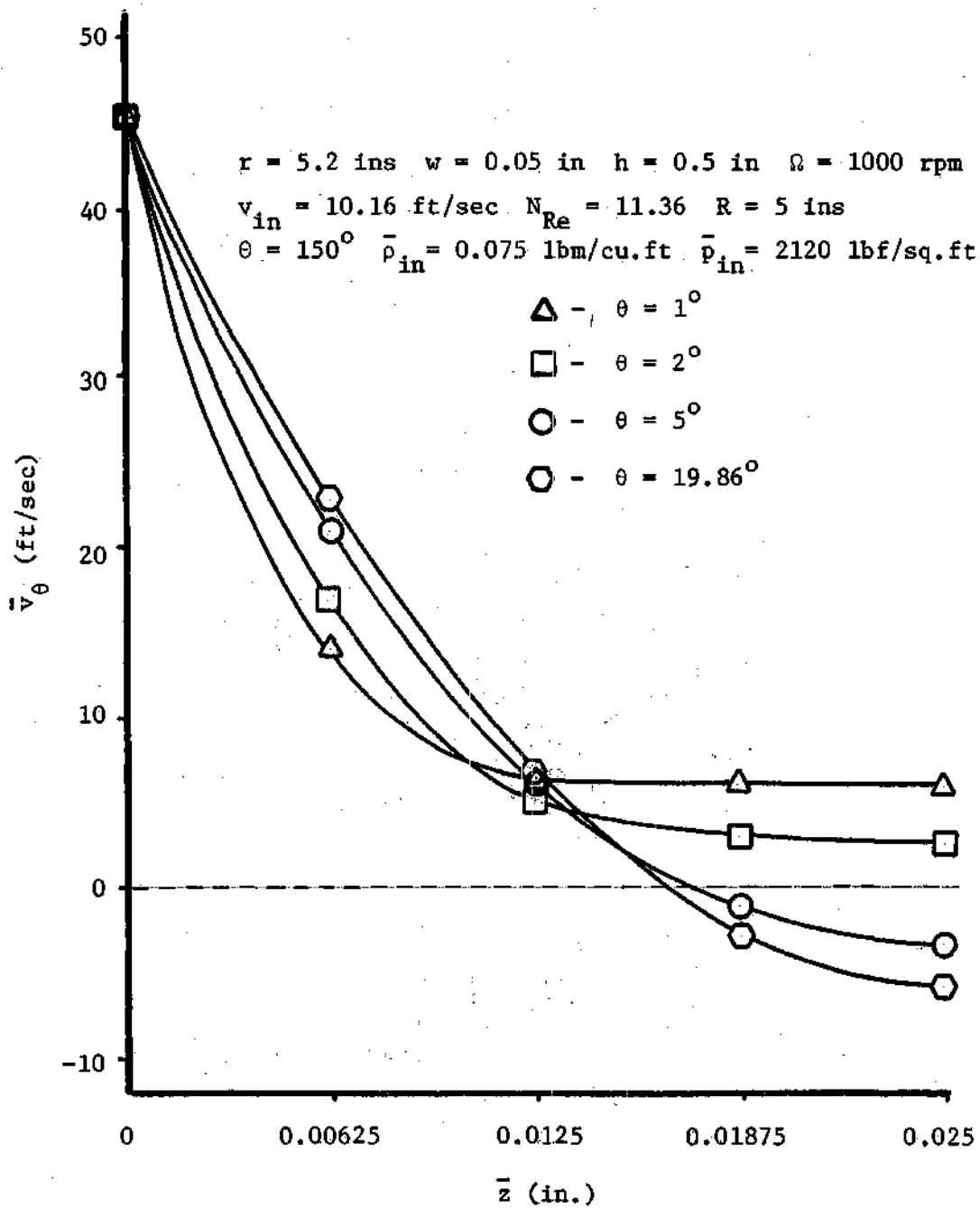Figure 9.   Tangential Velocity Profile Development

Figure 10. Tangential Velocity Profile Development

$w = 0.05$ in $h = 0.5$ in $\Omega = 1000$ rpm

$v_{in} = 10.16$ ft/sec $N_{Re} = 11.36$ $R = 5$ ins

$\theta = 150^{\circ}$ $\bar{\rho}_{in} = 0.075$ lbm/cu.ft $\bar{P}_{in} = 2120$ lbf/sq.ft
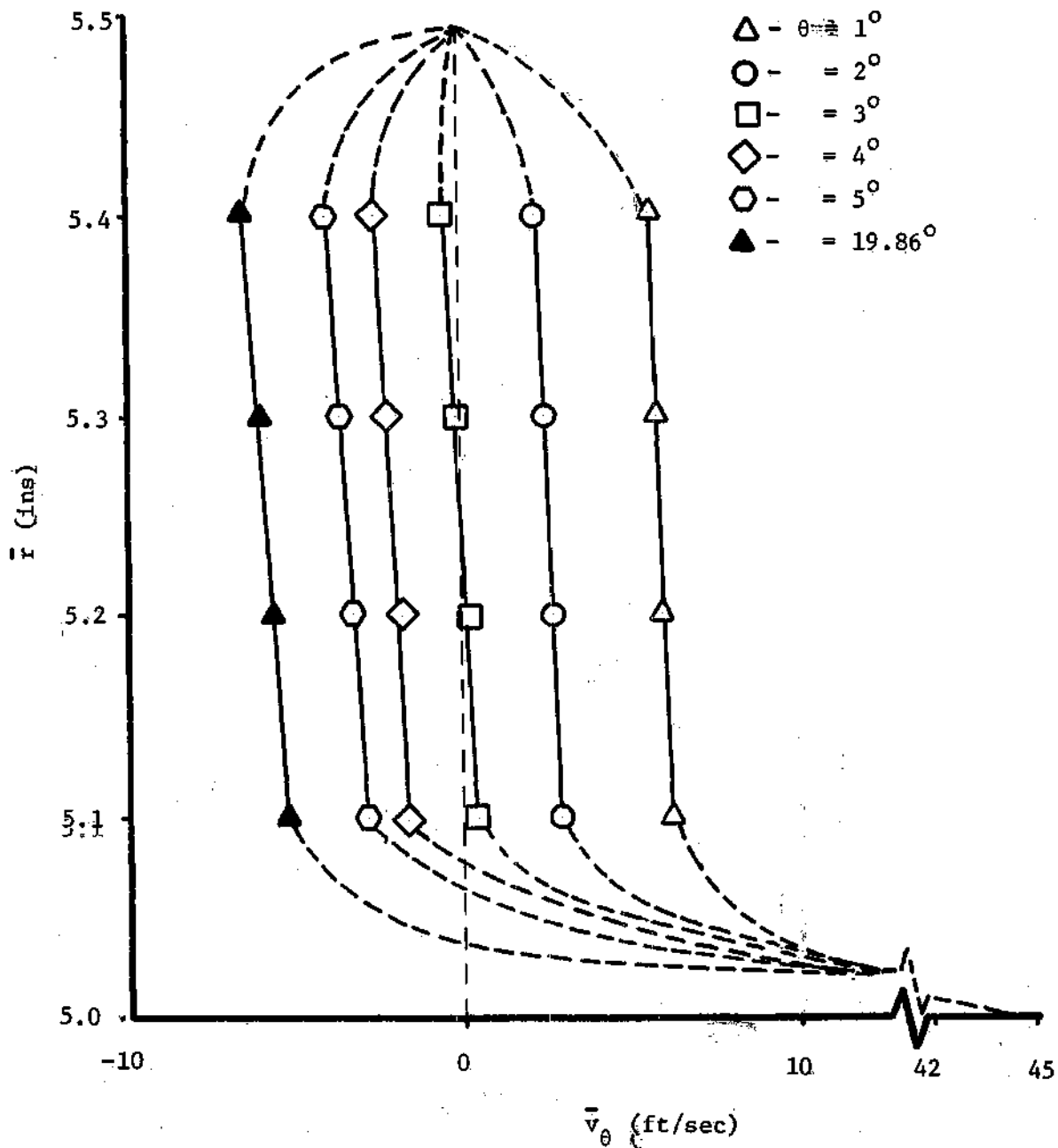
Figure 11.   Centerline Peripheral Velocity Development

of the aforementioned boundaries has been determined to be an order of magnitude less than the tangential shearing of the flow so it is not neeessary to incorporate these boundary conditions into the calculations. The radial gradient observed in the velocity profiles is due to the different wall speeds for each radial station. Also, the difference in radial gradient between 19.86 degrees and one degree is caused by the stronger retardation of flow. This is because at larger radii the centrifugal force fields develop higher pressure forces. One of the important results is the absence of any extraordinary curvature or development of the profiles. This verifies that the contribution of the term $(h/R)(1/N_{Re})(\partial^2 v_r / \partial z^2)$ is negligible. The term was retained in the calculations for mathematical compatibility.

Figures 12, 13, and 14 have been presented to give the reader a complete picture of the velocity components for the same run. Large positive (moving from centerline towards the wall) axial velocity components feed the boundary layer forming on the wall until the fully developed stage is reached. The negative axial velocity components that are observed initially close to the centerline swing to positive values as soon as the boundary layer limits reach these stations. Although the radial velocity components do not exist in the continuity equation, the coupled nature of the sets of equations relate it to other velocity components. When the axial velocities close to the centerline are negative
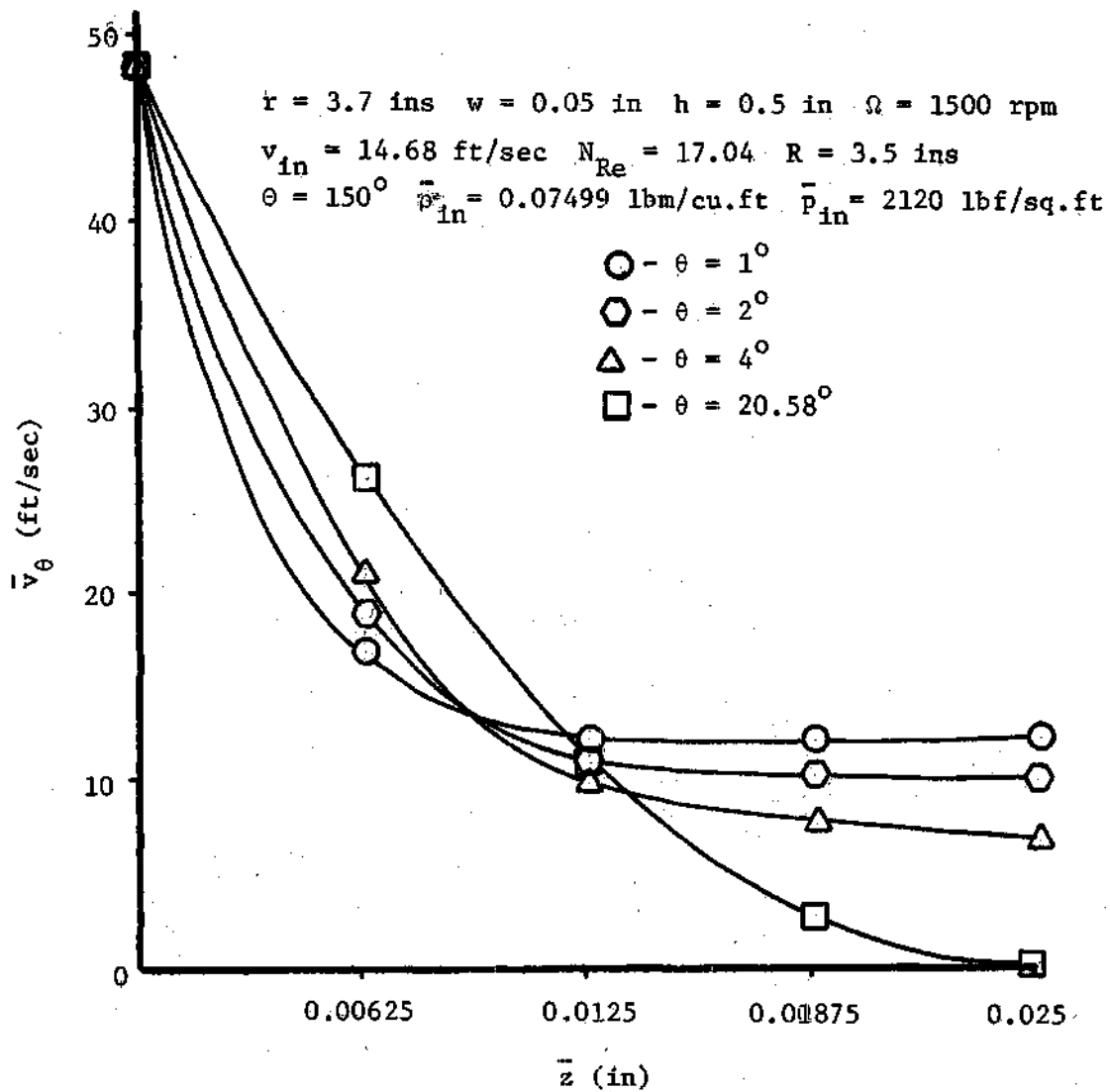
Figure 12. Tangential Velocity Profile Development

r = 3.7 ins   w = 0.05 in   h = 0.5 in Ω = 1500 rpm

v_{in} = 14.68 ft/sec N_{Re} = 17.04   R = 3.5 ins

Θ = 150° $\bar{\rho}_{in}$ = 0.07499 lbm/cu.ft $\bar{P}_{in}$ = 2120 lbf/sq.ft
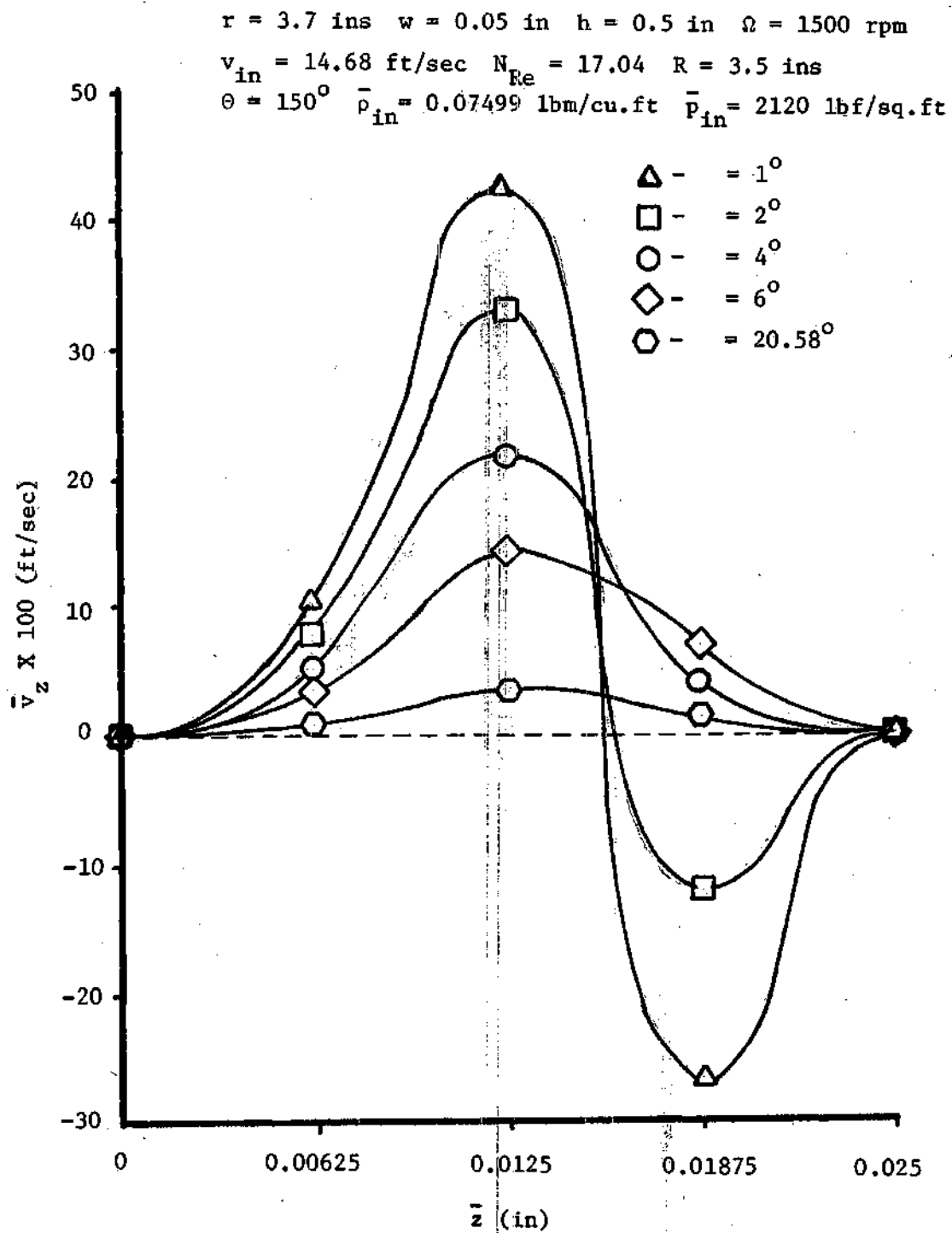
Figure 13.   Axial Velocity Profile Development

r = 3.7 ins   w = 0.05 in   h = 0.5 in Ω = 1500 rpm
v_{in} = 14.68 ft/sec N_{Re}= 17.04   R = 3.5 ins
θ = 150° $\bar{\rho}_{in}$= 0.07499 lbm/cu.ft $\bar{p}_{in}$= 2120 lbf/sq.ft

○ - θ = 1°
□ - θ = 2°
△ - θ = 4°
⬡ - θ = 6°
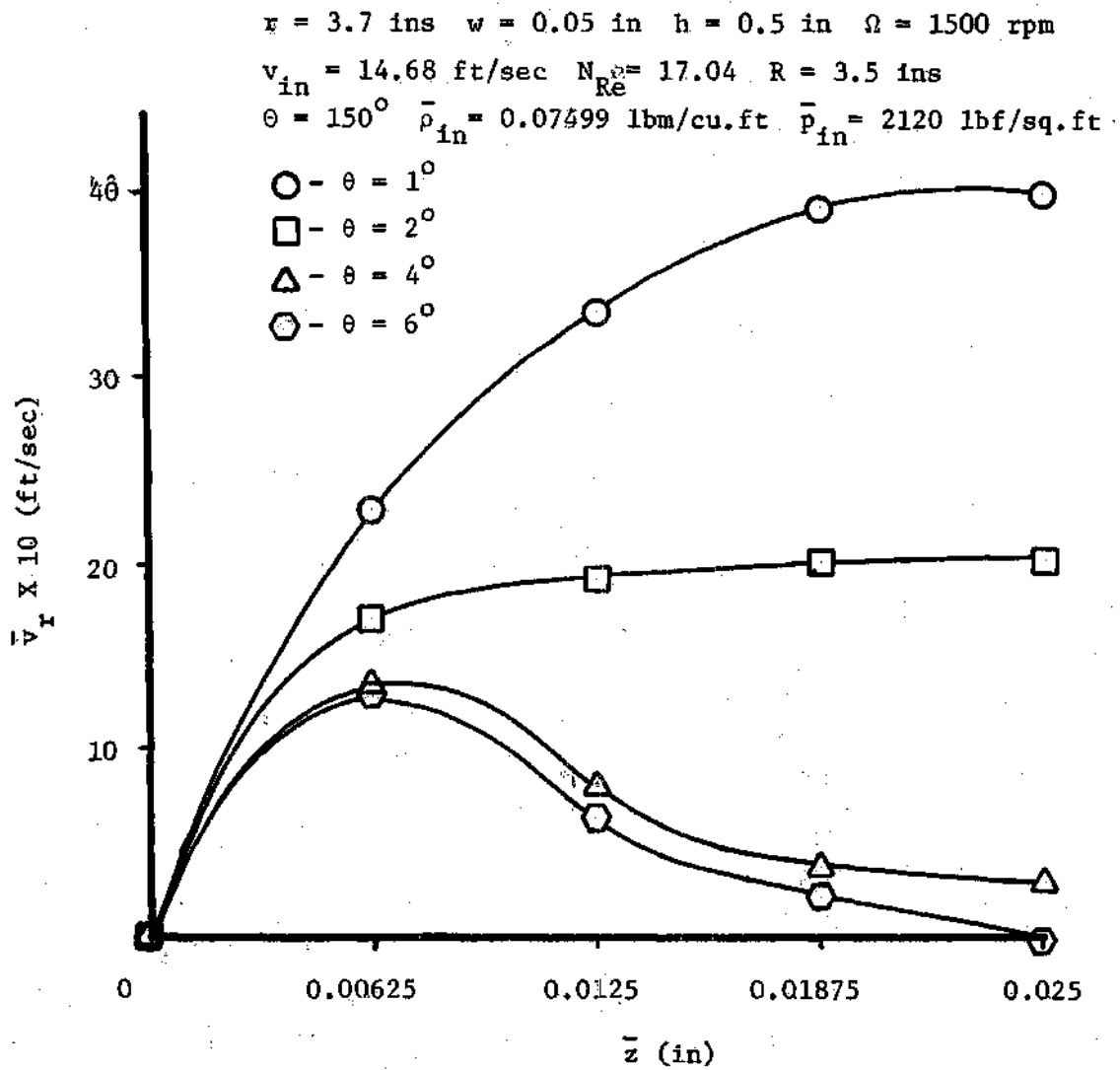
Figure 14.   Radial Velocity Profile Development

in Figure 13 note that radial velocities on Figure 14 maintain continuity by supplying radial flow into these regions of flow. The general tendency of the axial and radial velocity components is to approach small values. The values verify the initial assumptions concerning the orders of magnitude which were made during dimensional analysis.

As a result of the larger shearing of the fluid flow at the inlet section in all three cases plotted in Figure 15 the pressure gradients are larger at this section. Figure 16 illustrates the linear development at the fully developed section of the flow field. The tangential profile of pressures at the inlet section approaches fully developed behavior asymptotically. The change in curvature in pressure profile is observed on two of the runs in Figure 15. This is because of the partial peripheral flow reversal or stagnation at the same angular stations (see Figures 10 and 12) where the inflection in pressure profiles occur.

In Figures 17 and 18 radial pressure gradients at exit planes are shown. Figure 17 compares the radial gradients of flows with identical wheel tip speeds but different inlet velocities. Apparently, the radial pressure gradients are weakly influenced by the change in inlet velocities. However, as shown in Figure 18, higher tip speeds cause larger radial pressure gradients. Therefore, centrifugal force field is influenced stronger by increases in tip speeds rather than increases in inlet velocities.

w = 0.05 in   h = 0.5 in $\bar{\rho}_{in}$=0.07499 lbm/cu.ft $\bar{p}_{in}$=2119 lbf/sq.ft

△ – Ω = 1000 rpm v_{in}= 24.84 ft/sec   R = 5 ins
○ – Ω = 1500 rpm v_{in}= 14.68 ft/sec   R = 3.5 ins
□ – Ω = 1000 rpm v_{in}= 10.16 ft/sec   R = 5 ins

Figure 15.   Head Increase in Inlet Section

$$w = 0.05 \text{ in} \quad h = 0.5 \text{ in} \quad \bar{\rho}_{in}=0.07499 \text{ lbm/cu.ft} \quad \bar{P}_{in}=2119 \text{ lbf/sq.ft}$$

$\triangle$ - $\Omega = 1000$ rpm $\quad v_{in}= 24.84$ ft/sec $\quad R = 5$ ins

$\bigcirc$ - $\Omega = 1500$ rpm $\quad v_{in}=14.68$ ft/sec $\quad R = 3.5$ ins
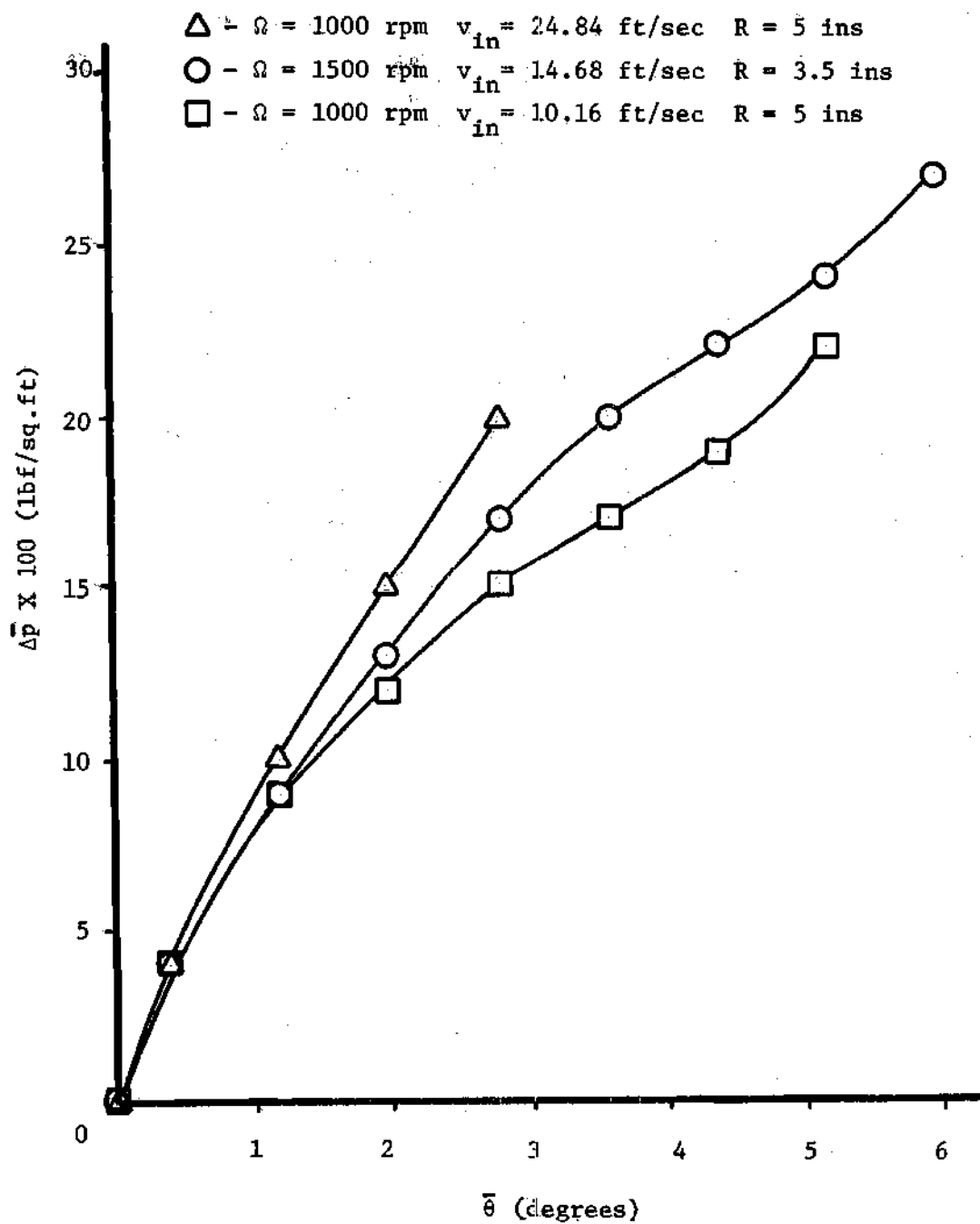
$\square$ - $\Omega = 1000$ rpm $\quad v_{in}= 10.16$ ft/sec $\quad R = 5.$ ins.
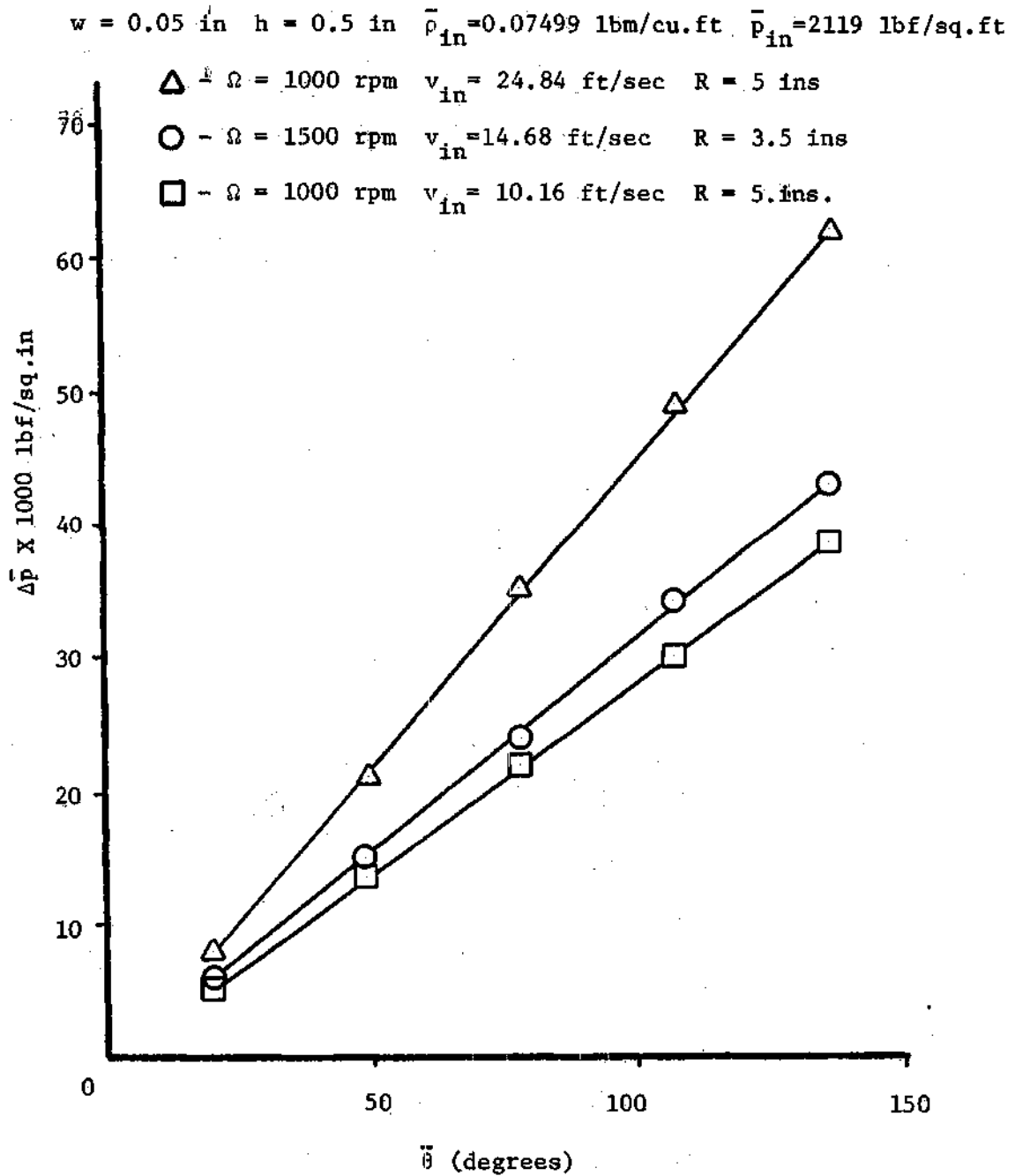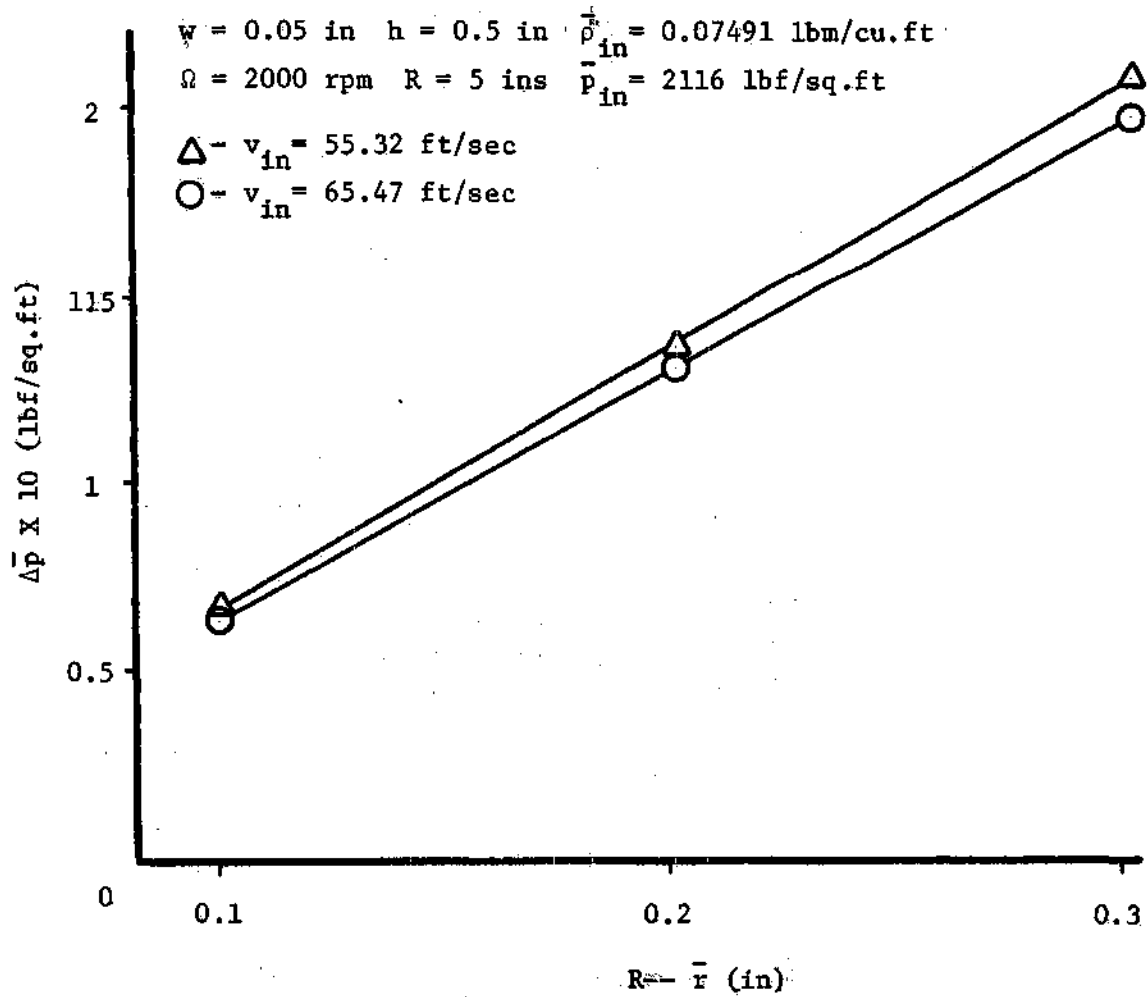
Figure 16. Head Increase Along the Periphery

Figure 17.   Radial Pressure Gradient at Exit Plane
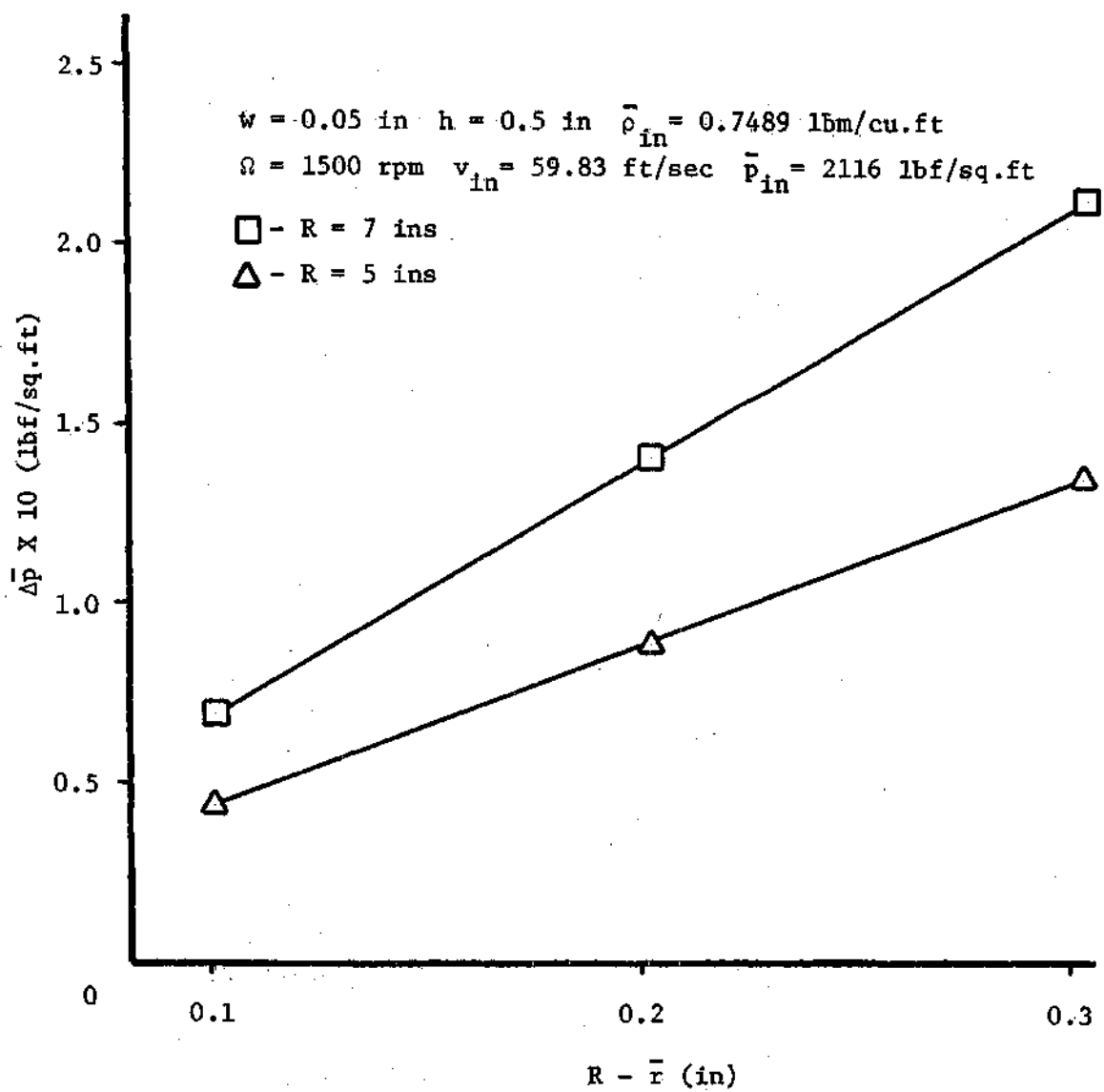
Figure 18. Radial Pressure Gradient at Exit Plane

Figures 19 and 20 show why varying tip speed is a more effective method of governing head rise. The steepness of the velocity gradients in Figure 20 imply that more shear work is imparted to the fluid particles as speed is increased to give them a higher pressure. In Figure 21 pressure developments for two different inlet flow rates are shown. At higher flow the pressure rise is decreased. The inverse proportionality between head rise and flow rate is common to all turbomachinery that require work input and is indicated by the figure.

The effects of changing tip speeds by changing either angular velocity or wheel radius on the flow are shown in Figures 22 and 23. Increasing tip speeds have shifted the head rise versus flow rate curves to the right in both cases meaning that for larger power inputs into the system higher pressure rises are expected for the same volume flow rate. However, the parallel nature of the constant wheel tip speed lines in Figure 23 is not observed in Figure 22. This can be explained as an effect of the change of centrifugal force fields when the radii are varied.

In Figure 24 the head-flow curve for N_{Re} = 17.03 and h/R = 0.1 is compared with Couette and Poiseuille flow. The defining equations are discussed in Appendix D. The striking correspondence between the Couette flow and the present analysis is illustrated. Perhaps insufficient grid spacing across the axis of the wheel led to inaccurate determination

$w = 0.05$ in $h = 0.5$ in $\bar{\rho}_{in} = 0.07489$ lbm/cu.ft

$\Omega = 1500$ rpm $v_{in} = 59.83$ ft/sec $\bar{p}_{in} = 2116$ lbf/sq.ft

△ - $R = 7$ ins

□ - $R = 5$ ins

$\Delta\bar{p} \times 1000$ (lbf/sq.in)

$\bar{\theta}$ (Degrees)
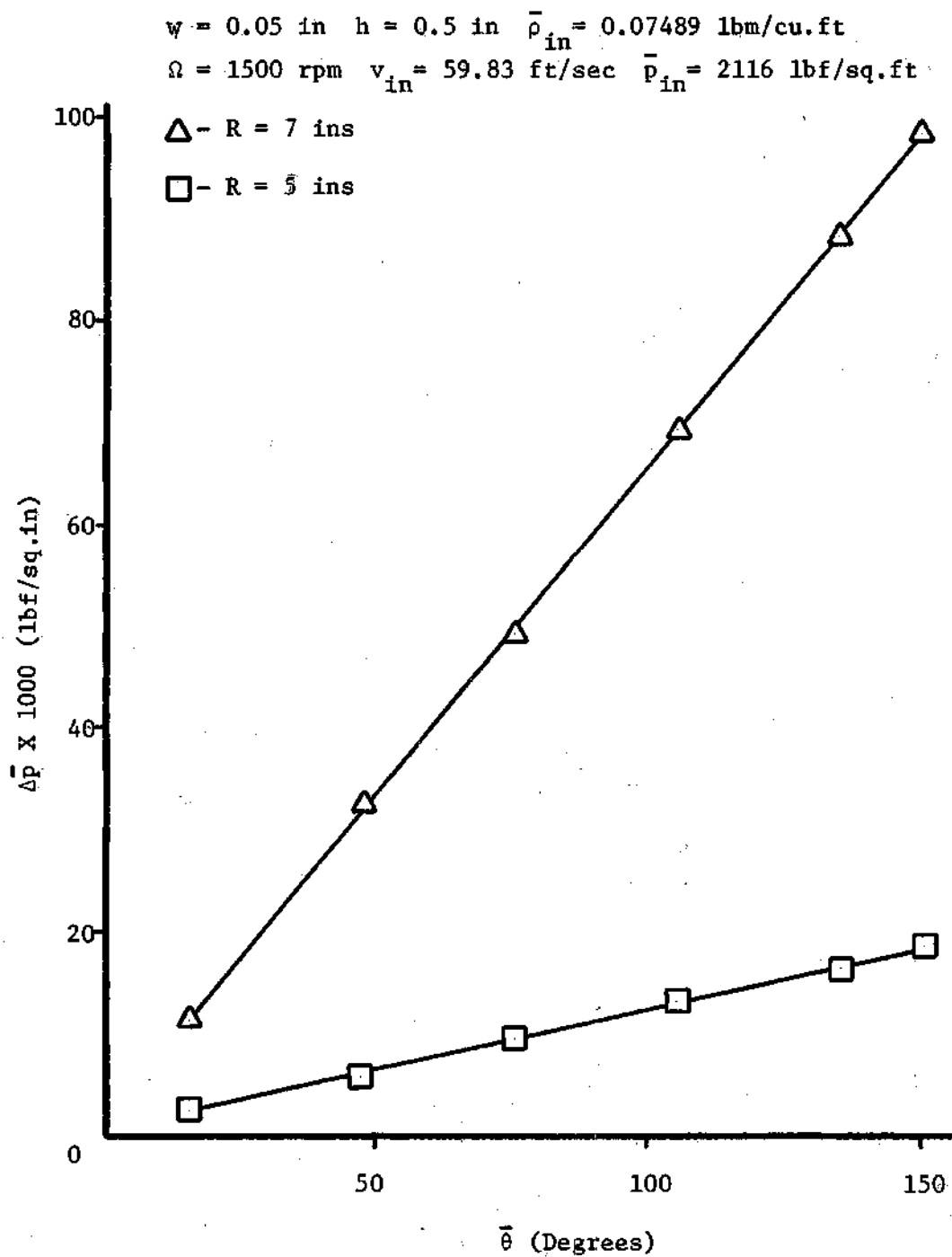
Figure 19.   Head Increase Along the Periphery
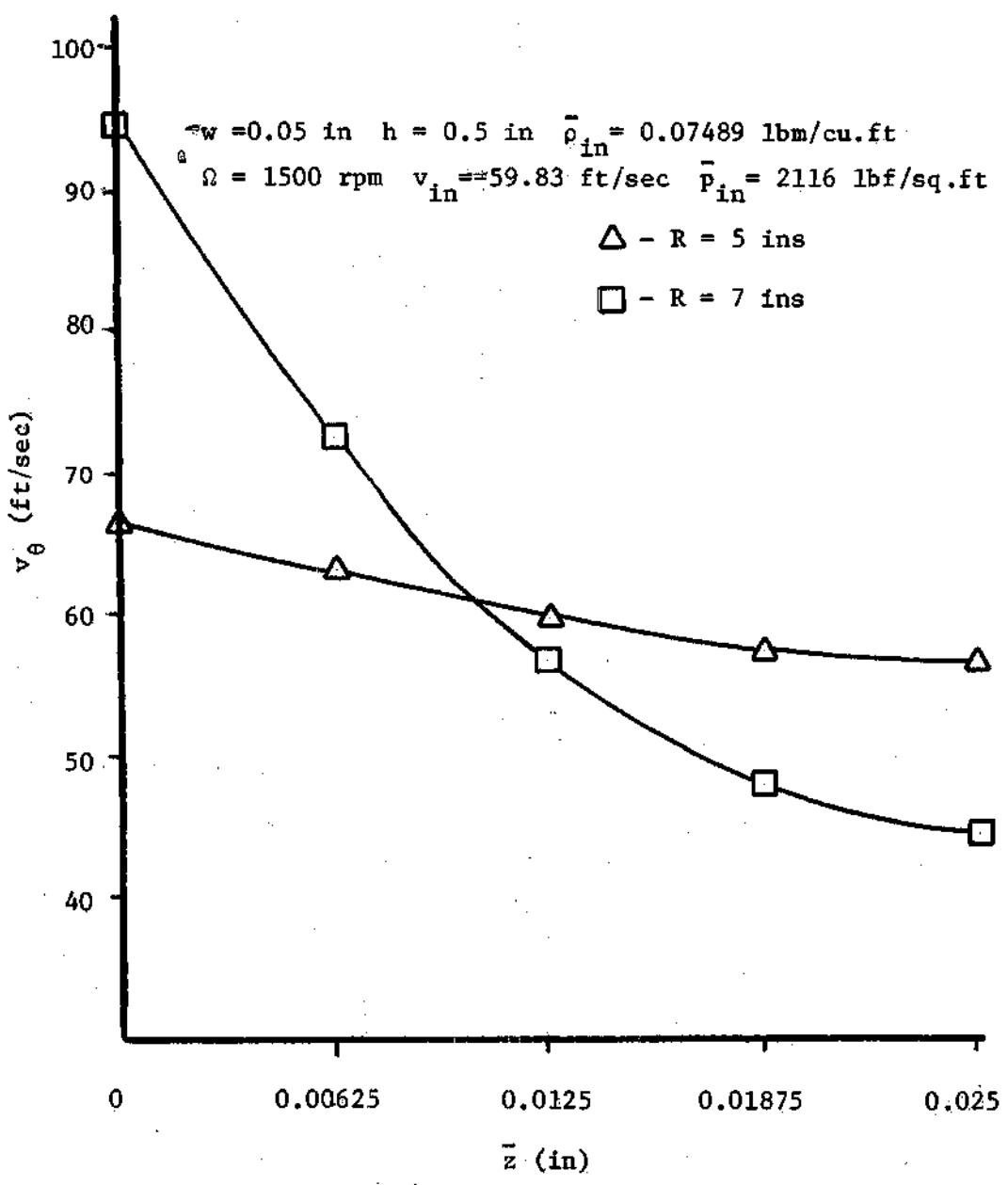
Figure 20. Exit Plane Peripheral Velocity Profiles
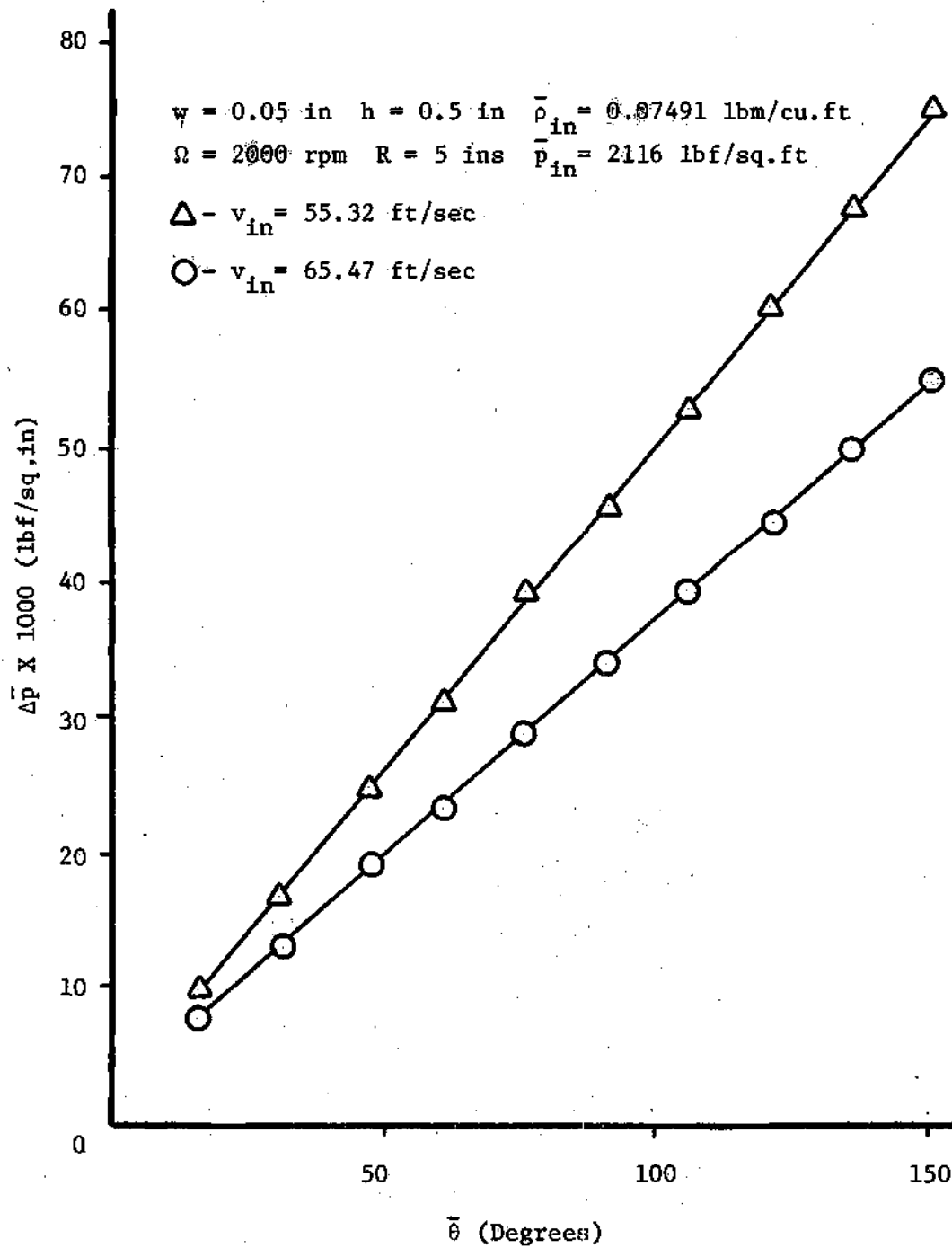
Figure 21.   Head Rise Along the Periphery of the Wheel
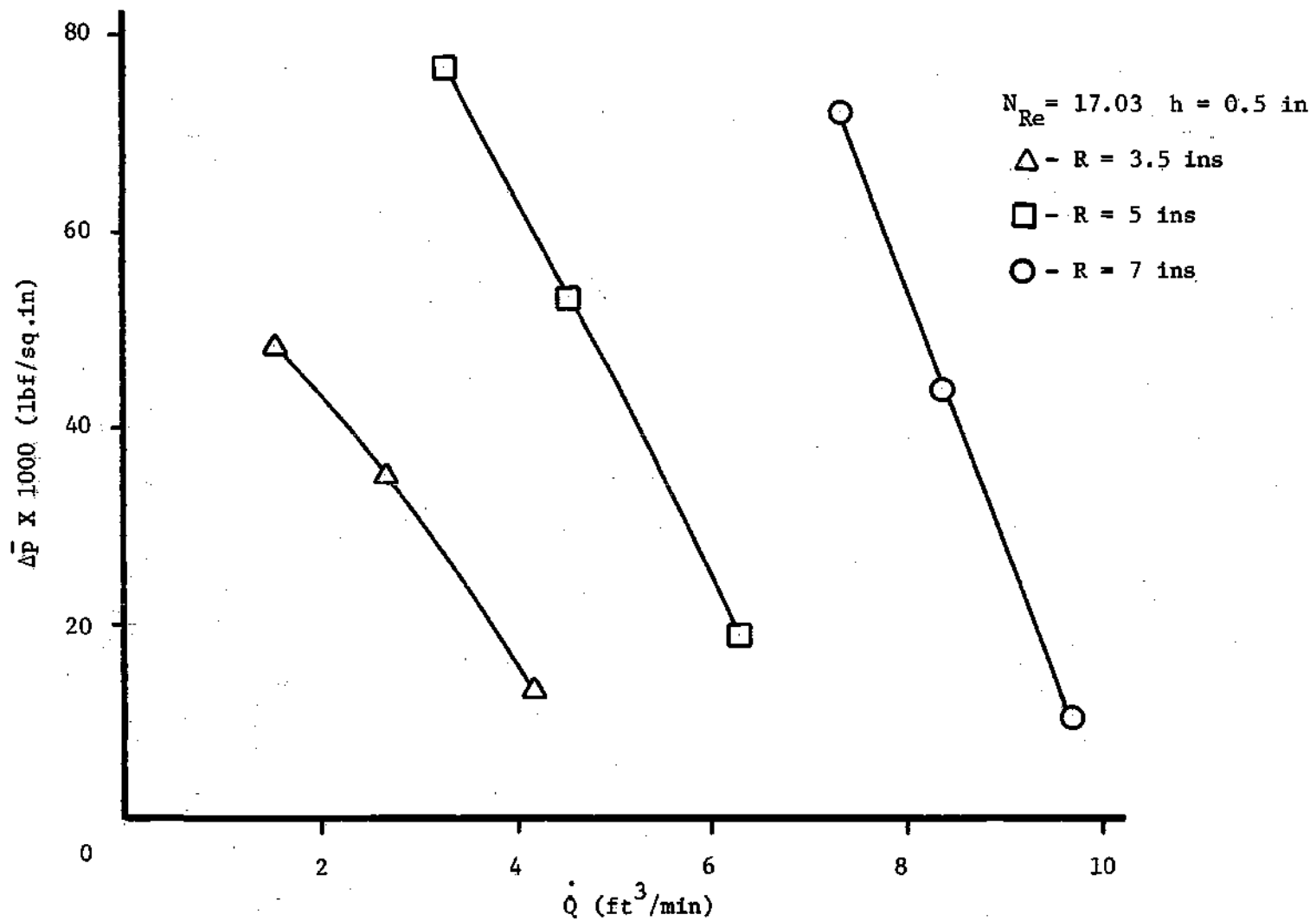
Figure 22. Head Versus Flow Curves for Different Wheel Radii
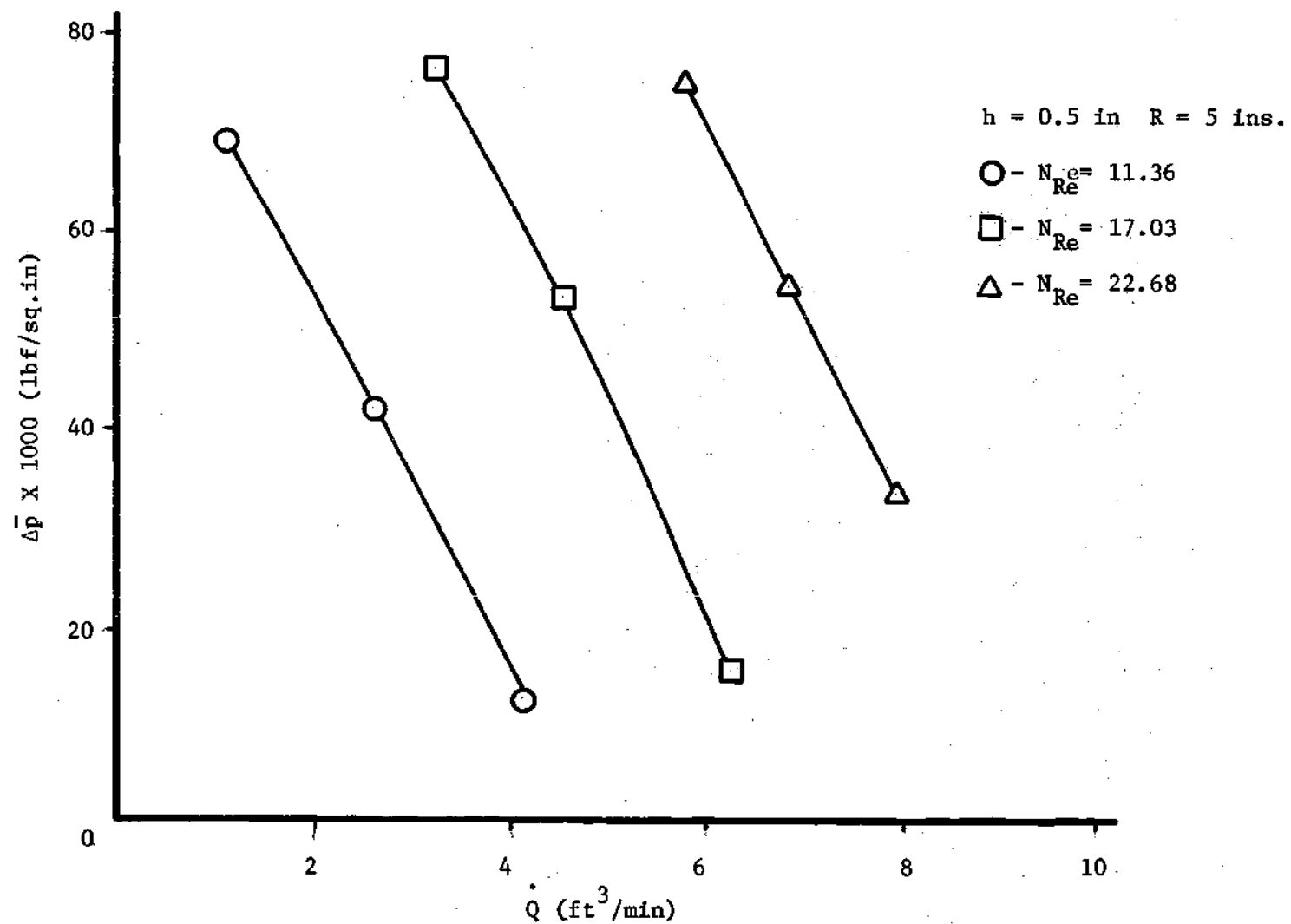
Figure 23. Head Versus Flow Curves for Different Rotational
Speeds of the Wheel
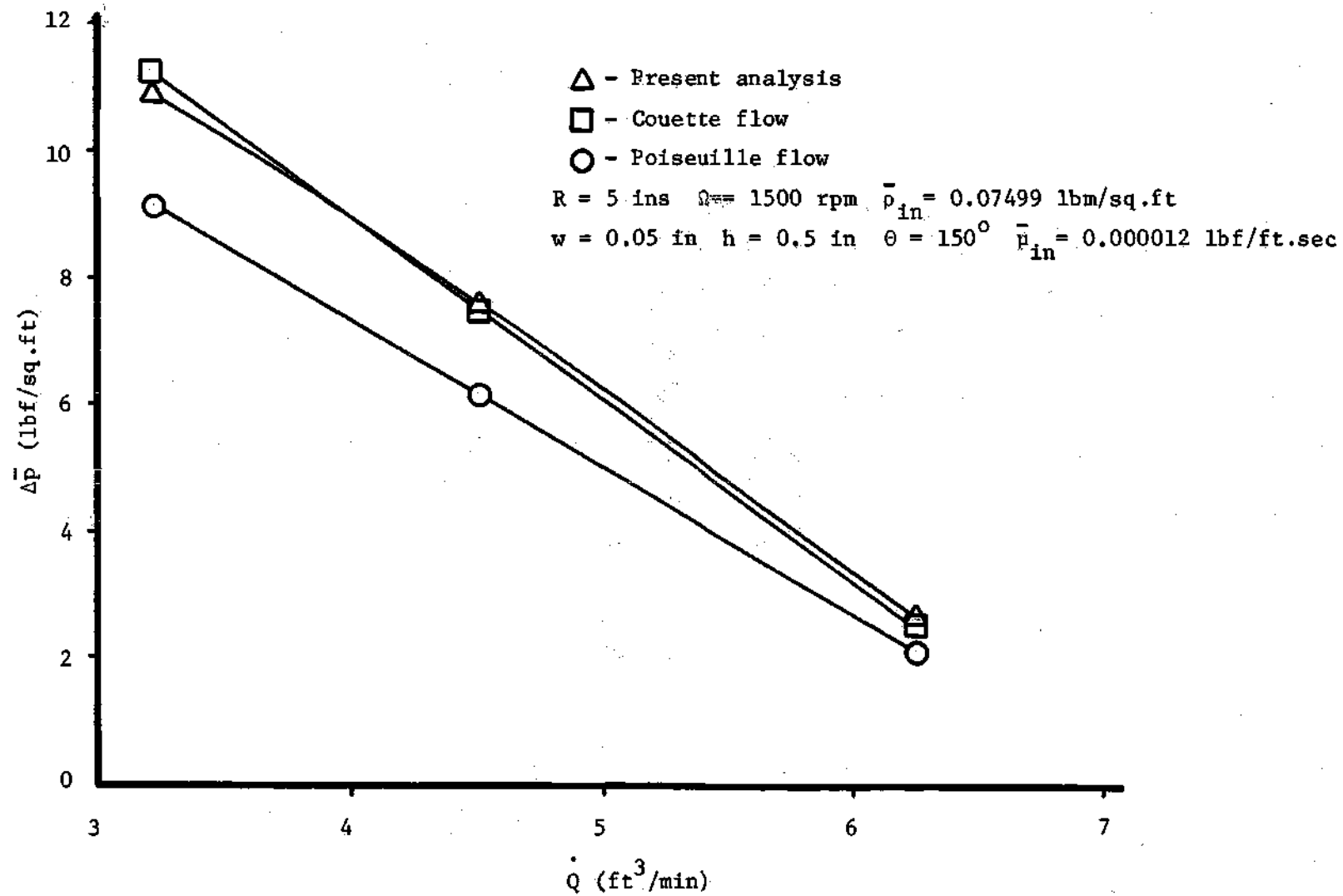
Figure 24. Head Versus Flow Curves of Couette, Poiseuille and Viscous
Drag Compressor Flow

velocity gradients across the axis and, consequently, agreement. Also the pressure gradients at the inlet section may not be large enough to affect the overall results. The difference between Poiseuille flow and this effort is probably a direct consequence of underestimation of the area exposed to shear in the hydraulic diameter. Apparently, the use of hydraulic diameter for laminar flow with high h/w geometries is misleading.

CHAPTER IV

CONCLUSIONS AND RECOMMENDATIONS

The results indicate that the governing equation can be treated by the mathematical techniques described in this paper to yield satisfactory solutions. The scope of the analysis is limited by certain geometrical constraints. If length ratios are not within the required orders of magnitude, the nature of the flow may change so drastically as to invalidate the set of equations used here.

A general conclusion is that for steady, incompressible, laminar flow, the overall compressor performance has Couette flow characteristics. This was an expected result since after fully developed profiles are established inertial force fields diminish and the flow becomes similar to that of a Couette flow by the nature of the defining equations. Due to rapid boundary layer development in the inlet section the higher head rises in the inlet do not have a great effect on overall performance. When the relative velocity between the fluid and moving walls is increased, boundary layer development requires a greater distance. The shearing effect of the stationery upper wall and moving lower wall have been eliminated as being an order of magnitude less than the shear on moving side walls. It is suspected that the stationery

upper wall will substantially effect the shearing of the fluid in its immediate vicinity. Further studies should be conducted to investigate this problem.

A double integration of peripheral velocity profiles at the point where the flow becomes fully developed gives a volume flow rate of 6-8 percent less than that at the inlet. The large amount of computations necessary to solve for the variables at each location in the flow field may lead to computer based truncation errors. Also the grid spacing or the exclusion of radial velocity gradients from the continuity equation on ground that they are small could be sources of error in the computed volume flow rate. Reference 7 suggests the use of an iterative method for determining the grid spacing. This method is based on checks of volume flow rate. The computer "Central Processing Unit" time necessary for this method is too costly.

An alternative method to minimize the effects of neglecting higher order Δ-quantities in the immediate neighborhood of the inlet is to improve the grid spacing in all three directions. The present grid points were spaced 0.00625 inch axially, 0.1 inch radially, and 0.2 degrees tangentially at the inlet section.

It has been observed that the centrifugal force field does not effect the system characteristics appreciably. Also the efficiency of the compressor for the laminar flow will be lower than what has been reported in References 5 and 6 for

experimental turbulent flow regimes. Velocity gradients close to the walls are much less than those under turbulent conditions.

The present analysis can be carried a step further by including compressibility effects into the analysis. Also further research must be conducted on the problem which covers heat transfer into the control volume. Then it would be possible to solve the problem using three dimensional Navier-Stokes equations in turbulent flow. A possible method could be to substitute eddy diffusivity terms into the governing equations.

APPENDICES

APPENDIX A

DERIVATION OF SIMPLIFIED CONTINUITY AND MOMENTUM
EQUATIONS BY DIMENSIONAL ANALYSIS

The governing equations as listed previously were,

Continuity:

$$\frac{1}{r} \left(\frac{\partial}{\partial \overline{r}} (\overline{r}\, \overline{v}_r) \right) + \frac{1}{\overline{r}} \left(\frac{\partial \overline{v}_\theta}{\partial \theta} \right) + \frac{\partial \overline{v}_z}{\partial \overline{z}} = 0$$

Momentum equations: r-direction,

$$\overline{\rho} \left(\overline{v}_r \frac{\partial \overline{v}_r}{\partial \overline{r}} + \frac{\overline{v}_\theta}{\overline{r}} \frac{\partial \overline{v}_r}{\partial \theta} - \frac{\overline{v}_\theta^{\,2}}{\overline{r}} + \overline{v}_z \frac{\partial \overline{v}_r}{\partial \overline{z}} \right) = - \frac{\partial \overline{p}}{\partial \overline{r}} + \overline{\mu} \left[\frac{\partial}{\partial \overline{r}} \left(\frac{1}{r} \frac{\partial}{\partial \overline{r}} (\overline{r}\, \overline{v}_r) \right) + \right.$$

$$\left. \frac{1}{\overline{r}^2} \frac{\partial^2 \overline{v}_r}{\partial \overline{\theta}^2} - \frac{2}{\overline{r}^2} \frac{\partial \overline{v}_\theta}{\partial \overline{\theta}} + \frac{\partial^2 \overline{v}_r}{\partial \overline{z}^2} \right]$$

θ-direction,

$$\overline{\rho} \left(\overline{v}_r \frac{\partial \overline{v}_\theta}{\partial \overline{r}} + \frac{\overline{v}_\theta}{\overline{r}} \frac{\partial \overline{v}_\theta}{\partial \overline{\theta}} + \frac{\overline{v}_r \overline{v}_\theta}{\overline{r}} + \overline{v}_z \frac{\partial \overline{v}_\theta}{\partial \overline{z}} \right) =$$

$$- \frac{1}{\overline{r}} \frac{\partial \overline{p}}{\partial \overline{\theta}} + \overline{\mu} \left[\frac{\partial}{\partial \overline{r}} \left(\frac{1}{\overline{r}} \frac{\partial}{\partial \overline{r}} (\overline{r}\, \overline{v}_\theta) \right) + \frac{1}{\overline{r}^2} \frac{\partial^2 \overline{v}_\theta}{\partial \theta^2} + \frac{2}{\overline{r}^2} \frac{\partial \overline{v}_r}{\partial \overline{\theta}} + \frac{\partial^2 \overline{v}_\theta}{\partial \overline{z}^2} \right]$$

z-direction,

$$\bar{\rho}(\bar{v}_r \frac{\partial \bar{v}_z}{\partial \bar{r}} + \frac{\bar{v}_\theta}{\bar{r}} \frac{\partial \bar{v}_z}{\partial \bar{\theta}} + \bar{v}_z \frac{\partial \bar{v}_z}{\partial \bar{z}}) = -\frac{\partial \bar{p}}{\partial \bar{z}} + \bar{\mu}[\frac{1}{\bar{r}} \frac{\partial}{\partial \bar{r}} (\bar{r} \frac{\partial \bar{v}_z}{\partial \bar{r}}) +$$

$$\frac{1}{\bar{r}^2} \frac{\partial^2 \bar{v}_z}{\partial \bar{\theta}^2} + \frac{\partial^2 \bar{v}_z}{\partial \bar{z}^2}]$$

The variables involved in these equations will be non-dimensionalized by dividing through constants that shall set the quotients to an order of magnitude of one.

$$r = \frac{\bar{r}}{R} \qquad \theta = \frac{\bar{\theta}}{\Theta} \qquad z = \frac{\bar{z}}{w} \qquad v_r = \frac{\bar{v}_r}{\Omega h} \qquad v_\theta = \frac{\bar{v}_\theta}{\Omega R}$$

$$v_z = \frac{\bar{v}_z}{\Omega w} \qquad \rho = \frac{\bar{\rho}}{\bar{\rho}_i} \qquad \mu = \frac{\bar{\mu}}{\bar{\mu}_i} \qquad p = \frac{\bar{p}}{\bar{\rho}_i \Omega^2 R^2}$$

Inserting the above non-dimensionalized variables in place of the dimensional ones yield the following set of equations:

Continuity equation,

$$\frac{\Omega h R}{R} \frac{\partial}{\partial r} (r\, v_r) + \frac{\Omega R}{\Theta} \frac{\partial v_\theta}{\partial \theta} + \frac{R \Omega w}{w} r \frac{\partial v_z}{\partial z} = 0$$

Remembering that h/R and w/R are very much less than one, the above equation reduces to,

$$\frac{1}{\Theta} \frac{\partial v_\theta}{\partial \theta} + r \frac{\partial v_z}{\partial z} = 0$$

r;momentum equation,

$$\overline{\rho}_i \rho (\frac{\Omega^2 h^2}{R} v_r \frac{\partial v_r}{\partial r} + \frac{\Omega^2 hR}{R\Theta} \frac{v_\theta}{r} \frac{\partial v_r}{\partial \theta} - \frac{\Omega^2 R^2}{R} \frac{v_\theta^2}{r} +$$

$$\frac{\Omega^2 wh}{w} \overline{v}_z \frac{\partial \overline{v}_r}{\partial z}) = - \frac{\overline{\rho}_i \Omega^2 R^2}{R} \frac{\partial p}{\partial r} + \overline{\mu}_i \mu [\frac{R\Omega h}{R^3} \frac{\partial}{\partial r} (\frac{1}{r} \frac{\partial}{\partial r} (r \ v_r)) +$$

$$\frac{\Omega h}{\Theta^2 R^2} \frac{1}{r^2} \frac{\partial^2 v_r}{\partial \theta^2} - \frac{\Omega R}{\Theta R^2} \frac{2}{r r^2} \frac{\partial v_\theta}{\partial \theta} + \frac{\Omega h}{w^2} \frac{\partial^2 v_r}{\partial z^2}]$$

Cancelling and rearranging,

$$\rho (\frac{h}{R} v_r \frac{\partial v_r}{\partial r} + \frac{1}{\Theta} \frac{v_\theta}{r} \frac{\partial v_r}{\partial \theta} - \frac{R}{h} \frac{v_\theta^2}{r} + v_z \frac{\partial v_r}{\partial z}) = - \frac{R}{h} \frac{\partial p}{\partial r} +$$

$$\frac{\mu}{\overline{\rho}_i \Omega hR} [\frac{h}{R} \frac{\partial}{\partial r} (\frac{1}{r} \frac{\partial}{\partial r} (r \ v_r)) + \frac{h}{\Theta^2 R} \frac{1}{r^2} \frac{\partial^2 v_r}{\partial \theta^2} - \frac{1}{\Theta} \frac{2}{r^2} \frac{\partial v_\theta}{\partial \theta} + \frac{hR}{w^2} \frac{\partial^2 v_r}{\partial z^2}]$$
$$\overline{\mu}_i$$

Selecting the largest components of the three major forces involved, i.e. inertial, pressure and viscous forces, also defining,

$$N_{Re} = \frac{\overline{\rho}_i \Omega w^2}{\overline{\mu}}$$

the equation above reduces to,

$$-\rho \; \frac{R}{h} \; \frac{v_\theta^2}{r} = - \; \frac{R}{h} \; \frac{\partial p}{\partial r} + \frac{\mu}{N_{Re}} \; (\frac{\partial^2 v_r}{\partial z^2})$$

The viscous forces have been retained although they are of order of magnitude less than the other two for mathematical compatibility.

θ-momentum equation,

$$\overline{\rho}_i \rho \, (\frac{\Omega^2 hR}{R} \, v_r \, \frac{\partial v_\theta}{\partial r} + \frac{\Omega^2 R^2}{\Theta R^2} \, \frac{v_\theta}{r} \, \frac{\partial v_\theta}{\partial \theta} + \frac{\Omega^2 hR}{R} \, \frac{v_r v_\theta}{r} + \frac{\Omega^2 wR}{w} \, v_z \, \frac{\partial v_\theta}{\partial z}) =$$

$$- \; \frac{\overline{\rho}_i \Omega^2 R^2}{\Theta R} \, \frac{1}{r} \, \frac{\partial p}{\partial \theta} + \overline{\mu}_i \mu [\frac{\Omega R^2}{R^3} \, \frac{\partial}{\partial r} \, (\frac{1}{r} \, \frac{\partial}{\partial r} \, (r v_\theta)) + \frac{\Omega R}{\Theta^2 R^2} \, \frac{1}{r^2} \, \frac{\partial^2 v_\theta}{\partial \theta^2} +$$

$$\frac{\Omega h}{\Theta R^2} \, \frac{2}{r^2} \, \frac{\partial v_r}{\partial \theta} + \frac{\Omega R}{w^2} \, \frac{\partial^2 v_\theta}{\partial z^2}]$$

Again, cancelling and reorganizing,

$$\rho (\frac{h}{R} \, v_r \, \frac{\partial v_\theta}{\partial r} + \frac{1}{\Theta} \, \frac{v_\theta}{r} \, \frac{\partial v_\theta}{\partial \theta} + \frac{h}{R} \, \frac{v_r v_\theta}{r} + v_z \, \frac{\partial v_\theta}{\partial z}) = - \; \frac{1}{\Theta} \, \frac{1}{r} \, \frac{\partial p}{\partial \theta} +$$

$$\frac{\mu}{\overline{\rho}_i \Omega R^2} \, [\frac{\partial}{\partial r} \, (\frac{1}{r} \, \frac{\partial}{\partial r} \, (r v_\theta)) + \frac{1}{\Theta^2 r^2} \, \frac{\partial^2 v_\theta}{\partial \theta^2} + \frac{h}{\Theta R} \, \frac{2}{r^2} \, \frac{\partial v_r}{\partial \theta} + \frac{R^2}{w^2} \, \frac{\partial^2 v_\theta}{\partial z^2}]$$
$$\overline{\mu}_i$$

Dropping smaller order terms and identifying N_{Re},

$$\rho\left(\frac{1}{\Theta}\frac{v_\theta}{r}\frac{\partial v_\theta}{\partial\theta} + v_z\frac{\partial v_\theta}{\partial z}\right) = -\frac{1}{\Theta}\frac{1}{r}\frac{\partial p}{\partial\theta} + \frac{\mu}{N_{Re}}\left(\frac{\partial^2 v_\theta}{\partial z^2}\right)$$

The above equation suggests that for efficient shearing action between the wall and the fluid particles the mechanical Reynolds number should not be so high as to minimize the contribution of shearing action to the pressure gradient in the compressor.

z-momentum equation,

$$\bar{\rho}_i\rho\left(\frac{\Omega^2 hw}{R}v_r\frac{\partial v_z}{\partial r} + \frac{\Omega^2 Rw}{R\Theta}\frac{v_\theta}{r}\frac{\partial v_z}{\partial\theta} + \frac{\Omega^2 w^2}{w}v_z\frac{\partial v_z}{\partial z}\right) =$$

$$-\frac{\bar{\rho}_i\Omega^2 R^2}{w}\frac{\partial p}{\partial z} + \bar{\mu}_i\mu\left[\frac{\Omega Rw}{R^3}\frac{1}{r}\frac{\partial}{\partial r}\left(r\frac{\partial v_z}{\partial r}\right) + \frac{\Omega w}{\Theta^2 R^2}\frac{1}{r^2}\frac{\partial^2 v_z}{\partial\theta^2} + \frac{\Omega w}{w^2}\frac{\partial^2 v_z}{\partial z^2}\right]$$

Again, cancelling and rearranging,

$$\rho\left(\frac{h}{R}v_r\frac{\partial v_z}{\partial r} + \frac{1}{\Theta}\frac{v_\theta}{r}\frac{\partial v_z}{\partial\theta} + v_z\frac{\partial v_z}{\partial z}\right) = -\frac{R^2}{w^2}\frac{\partial p}{\partial z} +$$

$$\frac{\mu}{\bar{\rho}_i\Omega wR}\bar{\mu}_i\left[\frac{w}{R}\frac{1}{R}\left(\frac{\partial}{\partial r}\left(r\frac{\partial v_z}{\partial r}\right)\right) + \frac{w}{\Theta^2 R}\frac{1}{r^2}\frac{\partial^2 v_z}{\partial\theta^2} + \frac{wR}{w^2}\frac{\partial^2 v_z}{\partial z^2}\right]$$

Cancelling smaller order terms yields,

$$\frac{\partial p}{\partial z} = 0$$

Similar procedures are applied to the boundary conditions. They have been listed previously.

APPENDIX B

A CHECK ON THE RESULTS USING A COUETTE FLOW ANALOGY

The moving boundaries of the slot create a Couette flow problem as illustrated below:
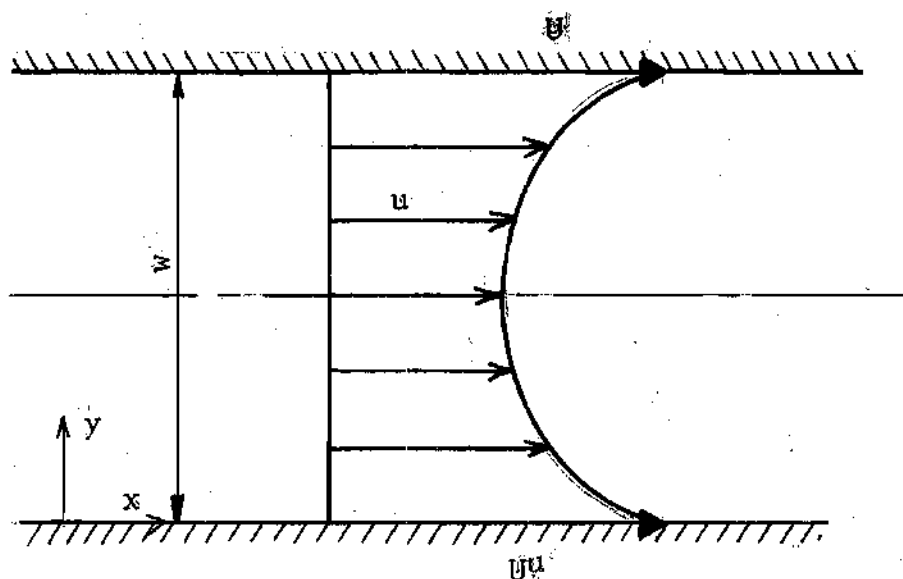
Figure 25. Couette Flow with Moving Boundaries

The governing equation for this flow

$$\frac{1}{2\overline{\mu}} \; g \; \frac{d\overline{p}}{dx} \; \frac{y}{w} \; (\frac{y}{w} - 1)w^2 + U = u$$

The results of a run with w = 0.05 inch, Ω = 1000 rpm and R = 5 inches have been compared with a Couette flow with

identical boundary conditions. At 150 degrees the centerline velocity (y/w = 0.5) was 15.51 ft/sec on the second radial station where R' = R + 2Δr = 5.2 inches when $\Delta\bar{p}$ was 5.33 psf. Couette flow with the same $\bar{\mu}$, $\Delta\bar{p}$, Δx, y/w, U and w has a centerline velocity of 18.1 ft/sec, a slightly higher value.

APPENDIX C

SELECTION OF MACH NUMBERS THAT YIELD
THE DESIRED INLET VELOCITIES

A test computer run was made to see which Mach numbers gave satisfactory inlet velocities. For this purpose the Mach number was varied by 0.001 increments from a value of 0.006 to 0.07. The output is reproduced in the table below.

Table 3. Inlet Velocities for Given Nozzle
Throat Mach Numbers

Mach No. $\times 10^3$	Flow Rate $\times 10^3$ (lbm/sec)	$v_\theta(1,j,k)$ (ft/sec)	Mach No. $\times 10^3$	Flow Rate $\times 10^3$ (lbm/sec)	$v_\theta(1,j,k)$ (ft/sec)
6	0.88	6.8	19	2.76	21.5
7	1.03	7.9	20	2.94	22.6
8	1.18	9.0	21	3.09	23.7
9	1.32	10.2	22	3.23	24.8
10	1.47	11.3	23	3.38	26.0
11	1.62	12.4	24	3.53	27.1
12	1.76	13.6	25	3.67	28.2
13	1.91	14.7	26	3.82	29.4
14	2.06	15.8	27	3.97	30.5
15	2.21	16.9	28	4.11	31.6
16	2.35	18.1	29	4.26	32.7
17	2.50	19.2	30	4.41	33.9
18	2.65	20.3	31	4.56	35.0
32	4.70	36.1	52	7.63	58.7
33	4.85	37.3	53	7.78	59.8
34	5.00	38.4	54	7.93	61.0
35	5.14	39.5	55	8.07	62.1
36	5.29	40.6	56	8.22	63.2
37	5.44	41.8	57	8.36	64.3
38	5.58	42.9	58	8.51	65.5
39	5.73	44.0	59	8.66	66.6
40	5.88	44.9	60	8.80	67.7
41	6.02	46.3	61	8.95	68.9
42	6.17	47.4	62	9.09	70.0
43	6.32	48.5	63	9.24	71.1
44	6.46	49.7	64	9.39	72.2
45	6.61	50.8	65	9.53	73.4
46	6.75	51.9	66	9.68	74.5
47	6.90	53.1	67	9.82	75.6
48	7.05	54.2	68	9.97	76.7
49	7.19	55.3	69	10.12	77.9
50	7.34	56.4	70	10.26	79.0
51	7.49	57.6			

APPENDIX D

DEVELOPMENT OF COUETTE FLOW AND POISEUILLE FLOW HEAD RISE FLOW RATE EQUATIONS

Appendix B contains the defining equation for Couette flow with moving boundaries. If this equation is integrated over the cross sectional area, a head rise flow rate relation for Couette flow will be obtained.

$$\iint_A \frac{1}{2\bar{\mu}} g_c \frac{d\bar{p}}{dx} \frac{y}{w} (\frac{y}{w}-1)w^2 dA + \iint_A U dA = \iint_A u dA$$

$$- \frac{d\bar{p}}{dx} \frac{hw^3 g_c}{12\bar{\mu}} + U wh = \dot{Q}$$

$$\Delta \bar{p} = \frac{12\mu\Delta x}{hw^3 g_c} (Uwh - \dot{Q})$$

For Poiseuille flow the defining equation of flow through a tube with boundaries moving at a velocity of U is,

$$u = - \frac{d\bar{p}}{dx} \frac{1}{4\bar{\mu}} (R^2 - r^2) + U$$

Integrating over the area of a circular pipe to get head rise-flow rate

$$\iint_A u \, dA = \iint_A -g_c \frac{dp}{dx} \frac{1}{4\mu} (R^2 - r^2) \, dA + \iint_A U \, dA$$

$$\dot{Q} = -\frac{\pi R^4}{8\overline{\mu}} g_c \frac{dp}{dx} + U \pi R^2$$

If the geometry is not circular, as in this case, the radius can be substituted by $D_H/2$ where D_H is the hydraulic diameter. However, since one wall is stationary the geometry of each slot is not readily represented by the hydraulic diameter for flow rate calculations. For simplicity the above equation is rearranged to eliminate hydraulic diameter dependence.

$$v_{in} = -\frac{D_H \, g_c}{32\overline{\mu}} \frac{d\overline{p}}{dx} + U \qquad \text{where } v_{in} \text{ is inlet velocity}$$

$$\Delta \overline{p} = (U - v_{in}) \frac{32\overline{\mu}}{D_H^2 \, g_c} \Delta x$$

Data presented in Figure 24 was obtained by inserting identical flow rate values in each of these equations and computing the head rises.

APPENDIX E

A SAMPLE DERIVATION OF FINITE DIFFERENCE

FORM OF θ-MOMENTUM EQUATION

Originally, the simplfied θ-momentum equation is in a partial differential equation form:

$$\frac{1}{\Theta} \frac{v_\theta}{r} \frac{\partial v_\theta}{\partial \theta} + v_z \frac{\partial v_\theta}{\partial z} = -\frac{1}{\Theta} \frac{\partial p}{r \partial \theta} + \frac{1}{N_{Re}} \left(\frac{\partial^2 v_\theta}{\partial z^2}\right)$$

All radial and axial derivatives are approximated by centered-finite-difference method whereas tangential derivatives use backward-finite difference approximation. The theory behind this method of approximating derivatives is Taylor series expansion of functions, discussed in References 11 and 12.

$$\frac{1}{\Theta} \frac{v_\theta}{r} \frac{\partial v_\theta}{\partial \theta} = \frac{1}{\Theta} \frac{v_\theta(i+1,j,k)}{r_j} \frac{v_\theta(i+1,j,k)-v_\theta(i,j,k)}{\Delta \theta}$$

$$v_z \frac{\partial v_\theta}{\partial z} = v_z(i+1,j,k) \frac{v_\theta(i+1,j,k+1)-v_\theta(i+1,j,k-1)}{2\Delta z}$$

$$-\frac{1}{\Theta} \frac{\partial p}{r \partial \theta} = -\frac{1}{\Theta} \frac{1}{r_j} \frac{p(i+1,j)-p(i,j)}{\Delta \theta}$$

$$\frac{1}{N_{Re}} \left(\frac{\partial^2 v_\theta}{\partial z^2} \right) = \frac{1}{N_{Re}} \left(\frac{v_\theta(i+1,j,k+1) - 2v_\theta(i+1,j,k) + v_\theta(i+1,j,k-1)}{(\Delta z)^2} \right)$$

Substituting the finite-difference approximations, the θ-momentum equation takes the following form:

$$\frac{1}{\theta} \frac{v_\theta(i+1,j,k)}{r_j} \frac{v_\theta(i+1,j,k) - v_\theta(i,j,k)}{\Delta \theta} + v_z(i+1,j,k)$$

$$\frac{v_\theta(i+1,j,k+1) - v_\theta(i+1,j,k-1)}{2\Delta z} = - \frac{1}{\theta} \frac{1}{r_j} \frac{p(i+1,j) - p(i,j)}{\Delta \theta}$$

$$+ \frac{1}{N_{Re}} \left(\frac{v_\theta(i+1,j,k+1) - 2v_\theta(i+1,j,k) - v_\theta(i+1,j,k-1)}{(\Delta z)^2} \right)$$

REFERENCES

1. Turbine-Compressor, G. T. Colwell and T. W. Jackson, United States Patent No. 3,751,908, August 14, 1973.

2. Turbine, Nikola Tesla, Official Gazette U. S. Patents No. 1061206 5/1913.

3. William Gordon, "An Investigation of a Disk Type Compressor," M.S. Thesis, 1962, Arizona State University, Tempe, Arizona.

4. W. Rice, "An Analytical and Experimental Investigation of Multiple-Disk Pumps and Compressors," Journal of Engineering for Power, Vol. 85, July, 1963, pp. 191-198.

5. S. Dusadeenoad, "Characteristics of a Viscous Flow Compressor," M.S. Thesis, Georgia Institute of Technology, September, 1970.

6. J. S. Caldwell, "Efficiency of a Viscous Flow Compressor," M. S. Thesis, Georgia Institute of Technology, June, 1973.

7. K. E. Boyd, W. Rice, "Laminar Inward Flow of an Incompressible Fluid Between Rotating Disks, with Full Peripheral Admission," Journal of Applied Mechanics, June, 1968, pp. 229-237.

8. H. Schlichting, Boundary-Layer Theory, Sixth Edition, McGraw-Hill Company, 1968.

9. G. K. Batchelor, An Introduction to Fluid Dynamics, Cambridge University Press, 1970.

10. A. H. Shapiro, The Dynamics and Thermodynamics of Compressible Fluid Flow, The Ronald Press Co., 1953.

11. P. J. Roache, Computational Fluid Dynamics, Hemmosa Publishers, 1972.

12. G. E. Forsythe, W. W. Wasow, Finite Difference Methods for Partial Differential Equations, Wiley, 1960.

13. D. D. Cracken, A Guide to FORTRAN IV Programming, John Wiley and Sons, 1972.

14. A. G. Cantrell, "Single Wheel Gas Turbine Computer Program," Georgia Institute of Technology, 1974.